POLITECNICO DI TORINO

Corso di Laurea Magistrale

in Ingegneria Aerospaziale

Tesi di Laurea Magistrale

Thermal modeling of Aerospace Electro-Mechanical Actuators for prognostic applications

Relatori

Prof. Ing. Paolo Maggiore

Prof. Ing. Matteo Davide Lorenzo Dalla Vedova

Candidato

Matteo Costarelli

Anno Accademico 2019/2020

Contents

Abstract

The More Electric Aircraft (EMA) and All Electric Aircraft (AEA) concepts consist in the elimination of all the on-board use of hydraulic, mechanical and pneumatic power. This approach promises to lower the total weight (electrical systems are generally much lighter than, for example, hydraulics due to the lack of hydraulic fluid), complexity, fuel consumption, operational costs and environmental impact of the aviation transportation segment. To fulfil this purpose, there is the need to replace or redesign those system that are currently relying on the above-mentioned types of power.

With this in mind, EMAs are one of the best solutions to operate Primary and Secondary Flight Controls, despite until now they have been mostly used for the latter, and other utilities like landing gear retraction, cargo bay opening, etc.). Basically, they consist in an electric Brushless DC motor with power electronics, paired with a mechanical transmission line linked to the prescribed surface.

Despite the advantages, as already been said, EMA are mostly used to operate secondary flight controls, due to lower reliability requirements and a certain unwillingness of aircraft manufacturers to employ a relatively “recent” technology: their fault mode are still not entirely known and higher reliability needed for primary flight control is preventing their full implementation. To close the gap with most used actuation system, a model based prognostic approach can be used to detect incipient failures of onboard EMA in order to improve safety and estimate the Remaining Useful Life (RUL).

In this work, it is proposed the implementation of a lumped parameter thermal model of a BLDC motor in the high detail dynamical model of an Electro-Mechanical Actuator. The model is developed in MathWorks *Simulink*/*Simscape* – *MATLAB* environment and validated via Finite Element Method thermal analysis (transient and stationary) in Autodesk Inventor NASTRAN environment.

Eventually the model is then tested under a set of different command input paired with different load and fault conditions to investigate the use of different output signal for future prognostic works.

1. Introduction

1.1 Overview

The purpose of this thesis is to create a simple thermal model in MATLAB / Simulink Environment of a typical Brushless DC motor used in an Electro-Mechanical actuator for aircraft flight controls to be integrated in a high-detailed model of the whole actuator. The model is capable of simulating the main faults occurring in a life of an EMA and can be used for the study of prognostic algorithms.

1.2 Flight Controls

The trajectory and attitude of an aircraft, i.e. the orientation of body axis relative to an external reference system, are controlled by creating local modifications of the aerodynamical forces through the variation of the exterior shape and geometry of the aircraft. These modifications produce unbalanced aerodynamic torques (M_{xB}, M_{yB}, M_{zB}) that changes the overall aerodynamic forces and so the aircraft attitude. Usually these torques are produced in a way that there is the least possible coupling between inputs (e.g. rudder deflection) and response non directly associated with that specific input (e.g. pitch).

On conventional aircraft, flight controls are divided into Primary Flight Control and Secondary Flight Control.

1.2.1 Primary Flight Controls

Primary flight controls are proportional and used to control the attitude of the aircraft by generating the already mentioned unbalanced torques. Pilots and/or Flight Control System need to constantly make changes to the attitude

in order to counterbalance disturbances or to modify the airplane trajectory. For this reason, the controls must have a band with a high upper limit for cutoff frequency, in order to have a responsive system. The loss of a primary flight control, without proper redundancy or backup mode, may lead into the loss of the aircraft.

Safety is an essential requirement for primary flight controls since the loss of flight controls, without proper redundancy or backup mode, may lead into the loss of the aircraft. Hence risk is minimized by increasing the reliability of a single component of the system or subsystem (decreasing the *probability* of a fault) designing the system to be fault-tolerant or providing the proper redundancy (decreasing the *severity* of the fault consequences).

On a conventional architecture aircraft, the primary control surfaces are:

- Rudder, to control Yaw about body Z-axis;
- Elevator, to control Pitch about body Y-axis;
- Ailerons, to control Roll about body Z-axis;

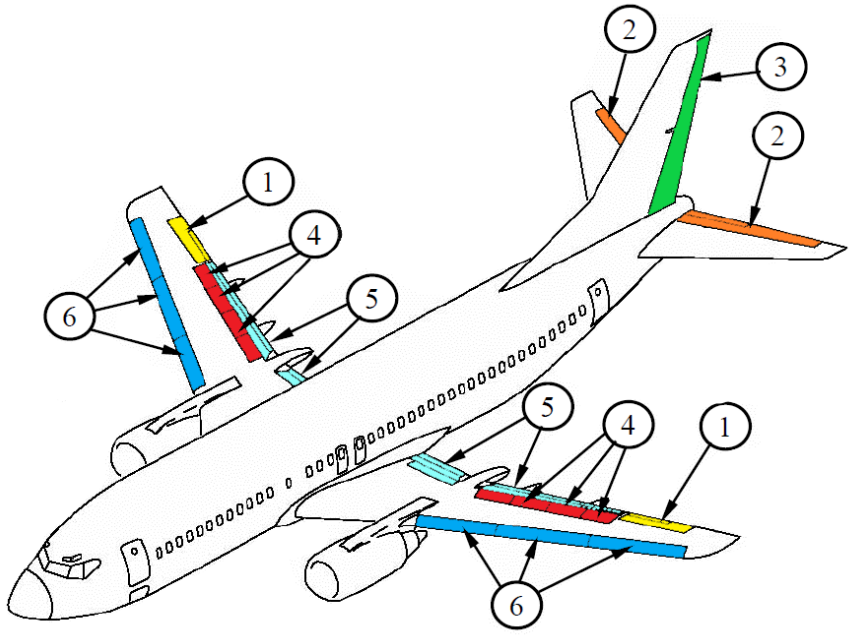

Figure 1.1 - Flight Control Surfaces on Boeing B-737 [1]

Flight controls can also by divided into *reversible* (or purely mechanical) and *irreversible*. The formers are usually found on smaller aircrafts and gliders: the pilot applies the force directly on the stick or pedals which is transmitted to the surfaces via pushrods and/or a cable and pulleys system. The latter are built on medium, large and on military aircrafts (due to increased flight speed) where the pilot power isn't enough to move the surface.

In order to compensate hinge torque, on irreversible flight controls, there is no need of pilot power, but electrical, hydraulic or mechanical power is used in replacement. Signal is transmitted separately in electrical (fly-by-wire) or optical (fly-by-light). In both of these types of command the pilot inputs a command through stick/pedals which is transduced by analog position sensors to an electrical signal, which is then managed by Flight Control Computer that, based on flight data (speed, acceleration, altitude, attitude, position of control surfaces, engine state, etc...), produces an output signal. This signal is then used by Power Supply Units of actuators to move the surface. During the process, position of the surface is always feedback to FCC, due to the presence of a position transducer, finally closing the control loop.

Advantages of fly-by-wire are weight reduction, easier maintenance (no rod, cables, pulleys, etc....), flight envelope protection, augmented stability and maneuverability due to more responsiveness of Flight Control System, reduction in fatigue stress on structures, enables Stability Augmentation System (SAS) and Control Augmentation Systems (CAS) to be used.

N°	Surface	Function	Type
1	Ailerons	Generate torque M_x	Primary
2	Elevator	Generate torque M_y	Primary
3	Rudder	Generate torque M_z	Primary
4	Spoiler (or flight spoiler)	Increase Drag, decrease Lift	Primary/Secondary
5	Trailing Edge high-lift devices	Increase Lift	Secondary
6	Leading Edge high-lift devices	Increase Lift	Secondary
7	Aerobrakes (or ground spoilers)	Increase Drag	Secondary

Table 1.1 - Flight Control Surfaces of Figure 1.1

Some of the drawbacks of powered actuation are the need of triple to quadruple redundancy to match the safety of a classic electromechanical actuation system (redundancy is intended both on actuators and on signal lines), the separation of the pilot's command from the direct feedback given by aerodynamical surfaces (the feedback is then given to the pilot via an Artificial Feel System),

Other non-conventional flight control surfaces may be found, usually on military fighter aircrafts. These surfaces aren't always only a primary flight control, since some works either as a primary or a secondary flight control.

- Flaperons (Flaps + Ailerons): the semi-wing trailing edge has a single moving surface that works either as a flap or as an aileron (e.g. F16). This is both a Primary and a Secondary Flight Control;
- *Canard*: delta wing aircraft might have a set of this horizontal control surfaces in front of the wing to control pitch in addiction to elevons (e.g. *Eurofighter*) or in addiction to elevator (e.g. *P-180*);
- *Elevons* (Elevator + Ailerons): usually used on delta wing aircraft with no horizontal stabilizer nor canàrd (e.g. *Mirage 2000*);
- *Tailerons* (Stabilizer + Ailerons): an example of Tailerons can be found on the *Tornado*. These surfaces are independent but might move symmetrically when needed as stabilizer/elevator;
- *"V-Tail"* (Elevator + Rudder): in "V-Tail" aircraft (*F-117A, F-22, F-35*) there is no distinction between the 3 conventional tail surfaces, there are 2 surfaces set at an angle lower than 90° with respect to the horizontal plane, so they can run simultaneously as rudders and as elevators.

1.2.2 Secondary Flight Controls

Secondary Flight Controls modify the flight characteristics (e.g. aerobrakes and spoiler increase C_{D0} value, flaps increase $C_{L,MAX}$), but unlike Primary Flight Controls they are in use only during a brief period of the mission (e.g. take-off, landing) or in some flight conditions. The second difference is that they aren't proportional to an input command but have a default set of positions. On conventional architectures we can find the following types of Secondary Flight Control:

- *Flaps*: they are located on the trailing edge of the wing and when activated they change the shape of the wing section, reducing the stall speed. Are only used during take-off and landing, since with an

increased lift we have also and increased drag, a decrease in aerodynamic efficiency, overall efficiency and range. The most common types of flaps are split flap, slotted flap and fowler flap;

- *Slats:* are found on the leading edge of the wing. They are set to create a by-pass flow from lower part of the airfoil to the upper part, increasing the velocity of the flow and preventing the stream to separate from the surface, therefore delaying the stall;
- *Spoilers and aerobrakes*: are located on the upper part of the surface. When opened they increase drag to rapidly reduce altitude without increasing speed; they are also used during landing after touch-down to initially reduce speed.

Secondary Flight Control have an intermittent duty-cycle, so there's no need to have a frequency band with a high upper limit since once deployed they maintain a stable position. Spoilers make an exception since they can be used to marginally control Roll at low speed.

Moreover, unlike primary flight control, they need to operate symmetrically with respect to the vertical plane of the aircraft. To achieve this type of operation they are actuated by a centralized power unit located at the wing-body intersection.

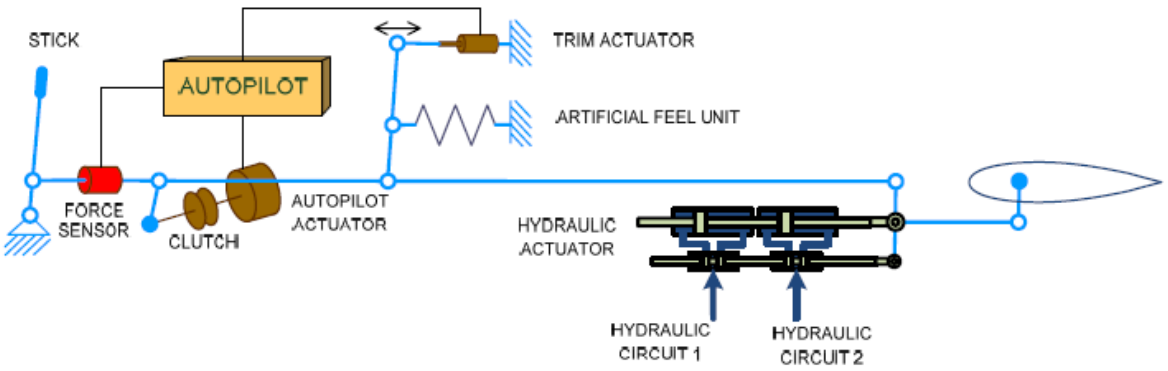

Figure 1.2 - Typical irreversible control system based on mechanically signaled hydraulic actuators.

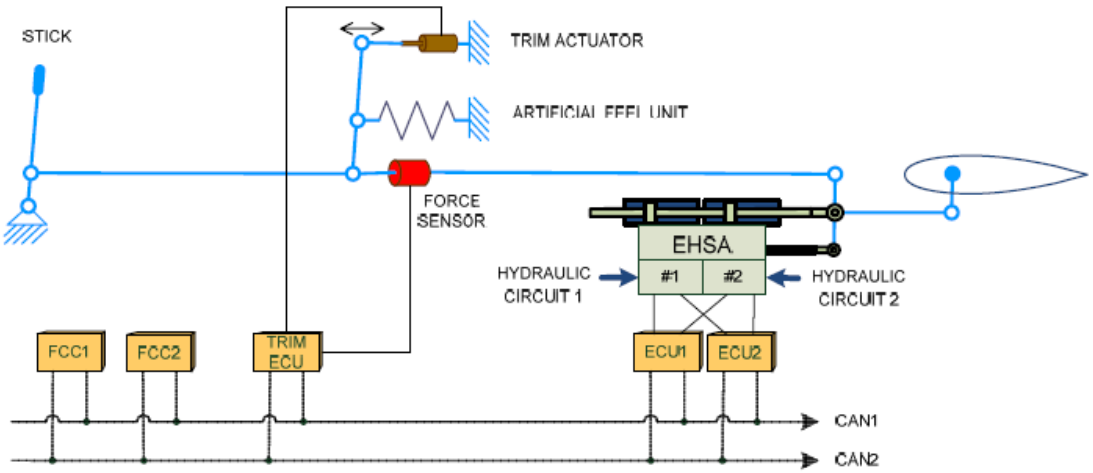

Figure 1.3 - Scheme of Fly-By-Wire system with mechanical redundancy

1.3 Actuation systems

Servomechanisms are usually utilized on aircrafts to actuate control surfaces. These systems generally measure their own output and force to rapidly and accurately follow the given command and could be designed to control almost all the physical quantities as position, speed, force, pressure, temperature or electrical magnitudes. A description of the mainly employed servomechanism follows.

1.3.1 Hydro-Mechanical Actuators

In hydromechanical actuators (Fig.4) the input signal is given by the pilot and applied through a linkage to the spool of a servo-valve. This is supplied with pressurized hydraulic fluid from aircraft hydraulic circuit at p_{mand}. The variation in node $x_t(t)$ position, makes the three-center *a-b* leverage rotate around the instantaneous center of rotation located at the end of the cylinder jack, thus opening the valve and creating a flow rate $Q_1(t)$. Finally, position of the jack is measured and mechanically subtracted, via the three-center lever, from the input signal. In this way, when the surface reaches commanded position, the servo-valve will automatically close itself. In this way the three-center lever is a mechanical proportional controller since it multiplies the

position error by a factor dependent by the lever geometry. This an old-fashioned solution and tend to be replaced by advanced and flexible systems,

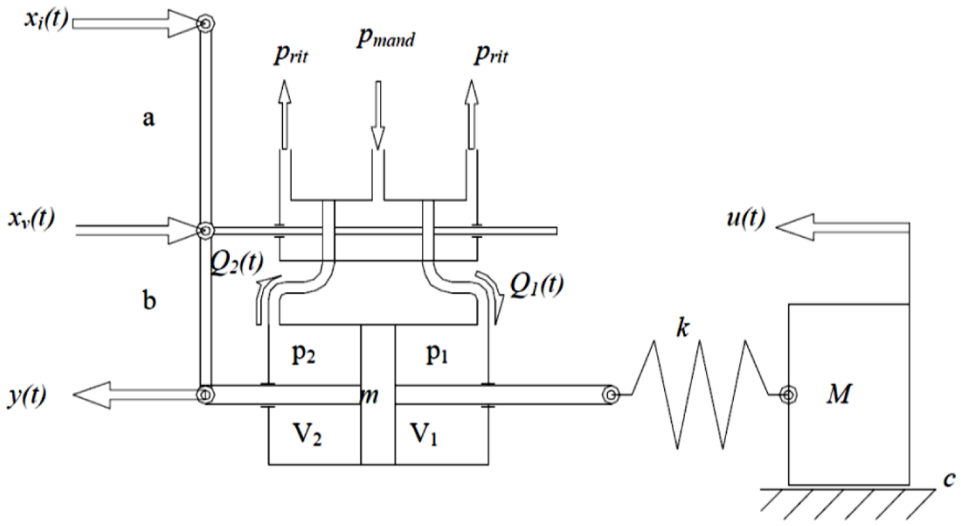

Figure 1.4 - Hydromechanical actuator scheme [1]

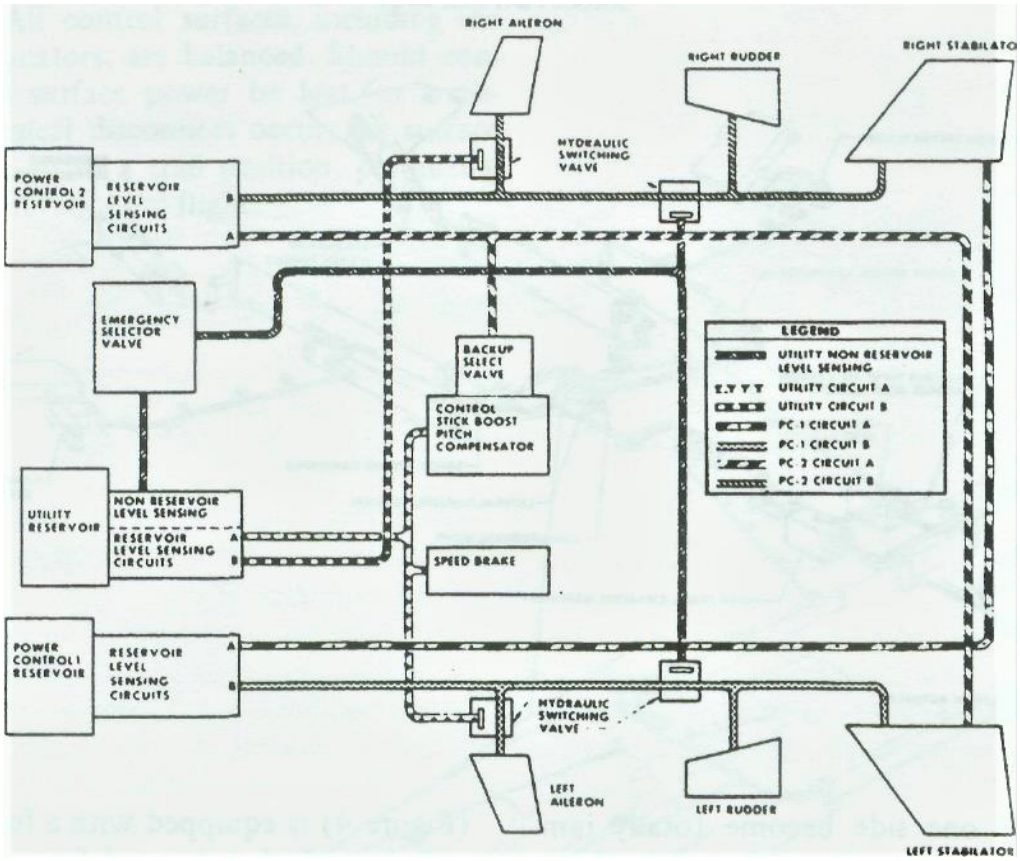

Figure 1.5 - Flight Control System Hydraulic Diagram [3]

but it's still installed on even some modern aircraft like Boeing B-737 and F-15 due to its accuracy and high reliability.

1.3.2 Electro-Hydraulic Actuators

This typology of actuators is in use on most modern civil and military; likewise the hydro-mechanical actuators, power is hydraulic (via pressurized fluid) but signal is provided by Flight Control Computer (fly-by-wire architecture) and not directly by pilot action. The component that regulates hydraulic oil is the servo-valve, which, in its simplest form laminates the fluid. Drawbacks with this typology of actuators are related to the leakage that consist in a loss of useful power and the constant monitoring of oil temperature to avoid polymerization.

The most commonly adopted system employs two stage flapper-nozzle servovalves, consisting in a electric torque motor moving the flapper, which is the first stage hydraulic valve. Pressure regulated by the flapper acts on the spool of the second stage valve, distributing pressure to the actuator jack. The spool position is fed back to the flapper mechanically through the feedback spring, while the piston position is measured by a Linear Variable Differential Transducer (LVDT) and transmitted to the control electronics.

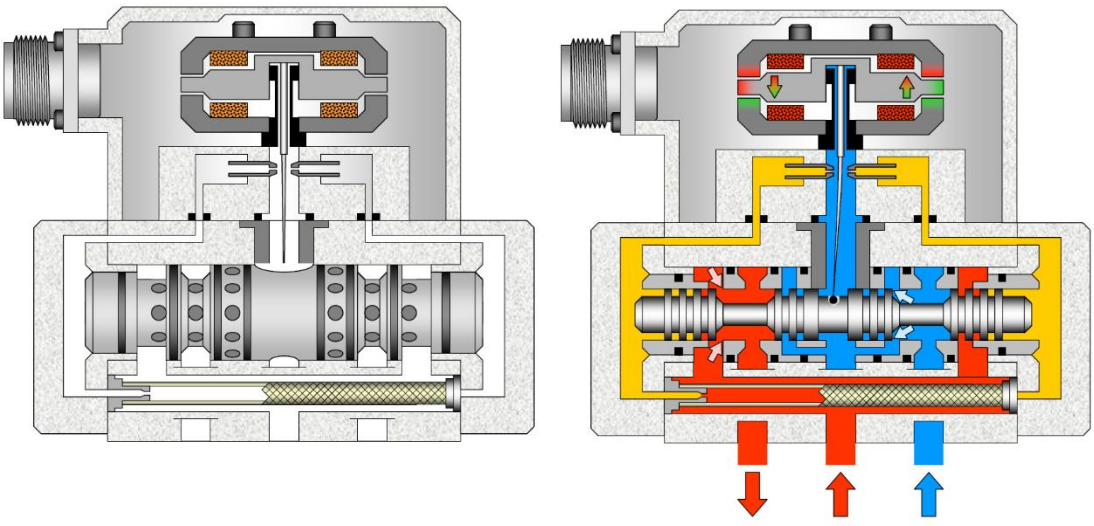

Figure 1.6 - A flapper nozzle servo-valve [1]

1.3.3 Electro-Hydrostatic Actuators (EHA)

The advantage of this relatively recent type of actuators is that it keeps the pressurized hydraulic fluid only in a limit area near the actuator and it eliminate the hydraulic signal transmission replacing it with an electric signal with advantages in terms of overall weight of the Flight Control system. This actuator is composed an electric machine that transform electrical power into mechanical power, an axial piston pump, to generate the controlled pressure and a linear (or rotary actuator).

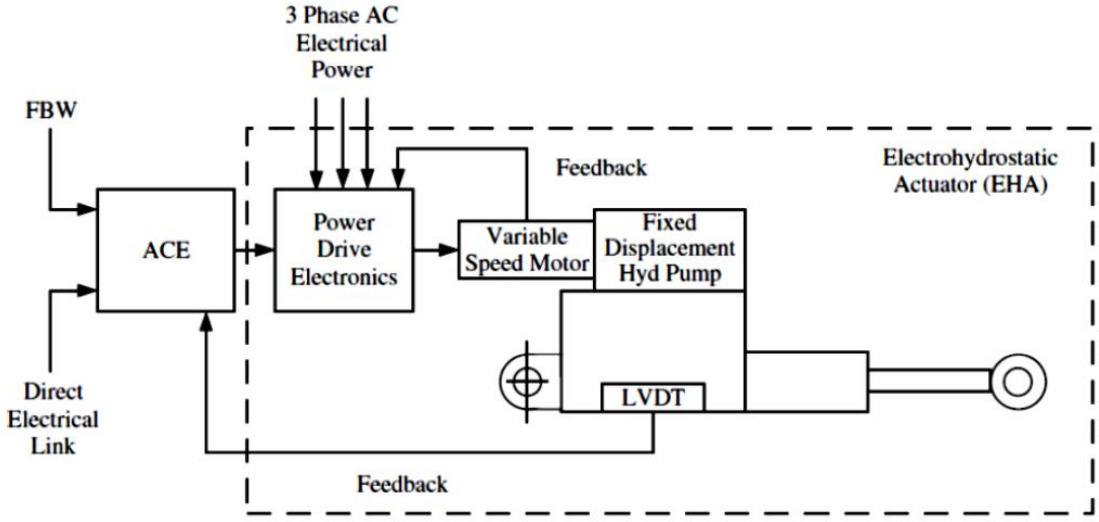

Figure 1.7 - EHA Scheme

Pilot's input and FCS input travel on the electrical cable of the fy-by-wire architecture, which is again lighter in term of weight with respect to an hydraulically driven signal transmission system. Another advantage other than reduced weight is the absence of friction losses or delays due to the flexibility typical of reversible mechanical control lines. The command given by the pilot (FBW signal in Figure 1.7) is than compared, in the ACE (Actuator Control Electronics), to a feedback signal measured by a Linear Voltage Differential Transducer LVDT (or a Rotary Voltage Differential Transducer RVDT). The error is then fed to the Power Drive Electronic). In this system the signal is amplified and, filtered from noises, is used to control the

actuation group. The PDE is supplied with a three phase AC power and uses the feedback of motor angular velocity to determine the exact amount of power needed. The actuation group consists in a variable speed motor (usually a Brushless DC) that drives an hydraulic pump and an actuator, that, finally controls the surface movement.

The advantages of having a localized hydraulic circuit is the high accuracy in position of the surface typical of hydro-mechanical actuators. EHA system is already being implemented in 5th generation military aircraft like F-22 and F-35 and in the Airbus A380, to operate primary control surfaces.

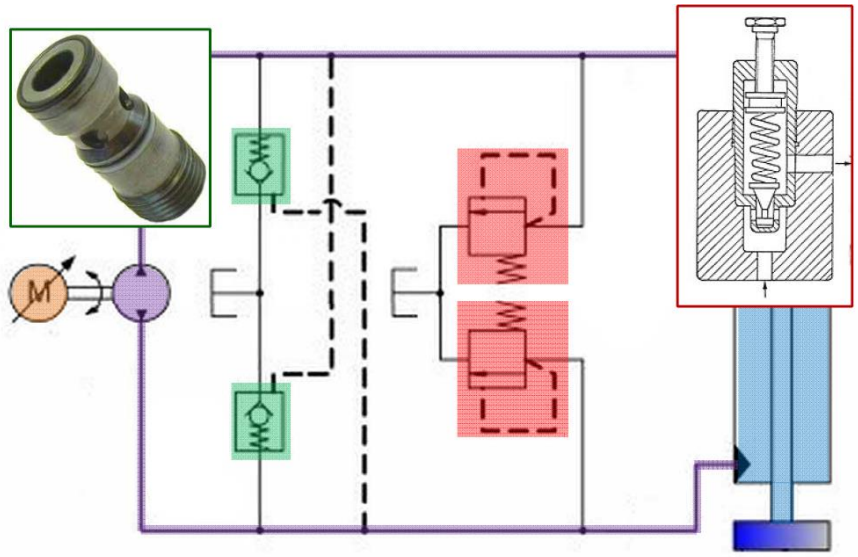

Figure 1.8 - EHA Hydraulic circuit [2]

1.3.4 Electro-Mechanical Actuators (EMA)

The step beyond the EHA is Electro-Mechanical Actuators that eliminate the need for the hydraulic circuit by means of gear reducer and/or a rotary-to-linear motion converter (a ball screw, jackscrew or a roller screw). As already been said EMAs are a lighter and simpler system compared to EHAs, but they are also a relatively recent technology and, to be used on primary flight control, their fault modes need to be completely studied. At this point in time their reliability is still lower than EHA and they cannot be certified for the use

for components and system that are critical for flight. Their use is confined to non-critical aircraft operations: e.g. secondary flight controls, landing gear retraction, cargo bay doors opening, etc... The only aircraft on which EMAs are being already used for primary flight controls are small-medium UAVs where the use of an onboard hydraulic system would be impractical.

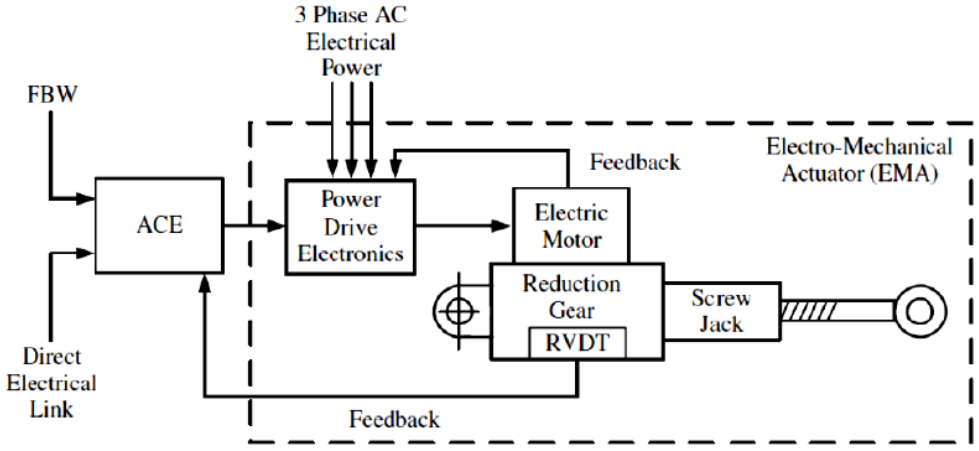

Figure 1.9 – Typical EMA Schematic [2]

A typical EMA is composed by the following components:

- ACE, Actuator Control Electronics: an electronic control unit where the logic is comparing feedbacks from the sensor to commands from the FCS through FBW;
- PDE, Power Drive Electronics module consisting in a static power converter, needed to transform direct current into three-phase alternating current for operating the motor;
- BLDC, Brushless DC;
- A transmission to reduce motor angular speed and increase its torque;
- A device to transform rotary motion into linear displacement of a component: usually this task is performed by a ball screw or a roller

screw, which are preferred to a lead screw for their better efficiency and higher specific maximum load.

- a position transducer, usually an LVDT, to measure the user displacement and transmit it to the controller.

Consiedering the transmission ratio as following:

$$\tau = \frac{\dot{\theta}_m}{\dot{\theta}_u} = \frac{1}{\eta_m}\frac{T_u}{T_m}$$

being $\dot{\theta}_m$ and T_m the motor angular speed and torque, $\dot{\theta}_u$ and T_u are the "user" angular speed and torque and η_m the transmission mechanical efficiency.

On these types of actuators, a high transmission ratio is needed in order not to use an oversized motor that needs even in that case to convert its high RPMs to useful torque to counterbalance surface loads. Typical motor speed rating is about from thousands to tens of thousand of rpm, while the required speed of a slow shaft of flight control surface is about tens of degrees per second. This requirement is typically expressed in angular terms (e.g. 50-60°/s on primary flight commands and 5-6°/s on secondary flight commands [2]).

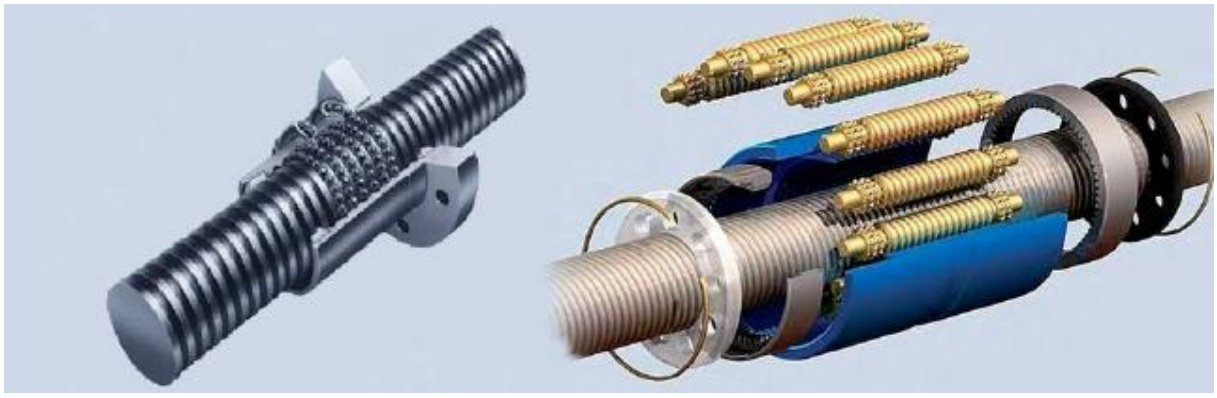

Figure 1.10 - A ball screw on the left and roller screw on the right

The rotary to linear motion conversion is performed by a all screw or a roller screw. These devices are usually composed by a high precision screw and the

transmission of motion is performed by a rolling component: the spheres inside the nut circuit in the ball screw and the satellite rollers in a roller screw. Compared to other rotary-to-linear transmission devices such as lead screw; they grant an increased efficiency due to absence of dry friction in favour of rolling resistance. The type of friction forces involved in the motion transmission directly implies a lower wear of mechanical parts, due to lower stress acting on the components.

The disadvantages of having an electric motor driven transmission is their difficulty to keep a fixed position with external load applied (i.e. delivering high torque in a near to near to zero velocity). A motor in this situation tries to deliver a torque by powering always the same phases, resulting in winding overheating and insulating material melting. With an irreversible transmission these problems can be overcame, with the downside that, in case of actuator failure, a backup actuator or the air stream cannot move the gripped surface. Therefore, a system for disconnecting the screw from the motor-reducer assembly would be required, increasing weight, cost and complexity. A solution to the problem might be the use of a new type of stepper hybrid stepper motor, that are able to output a controlled torque at zero speed.

2. Brushless DC motors

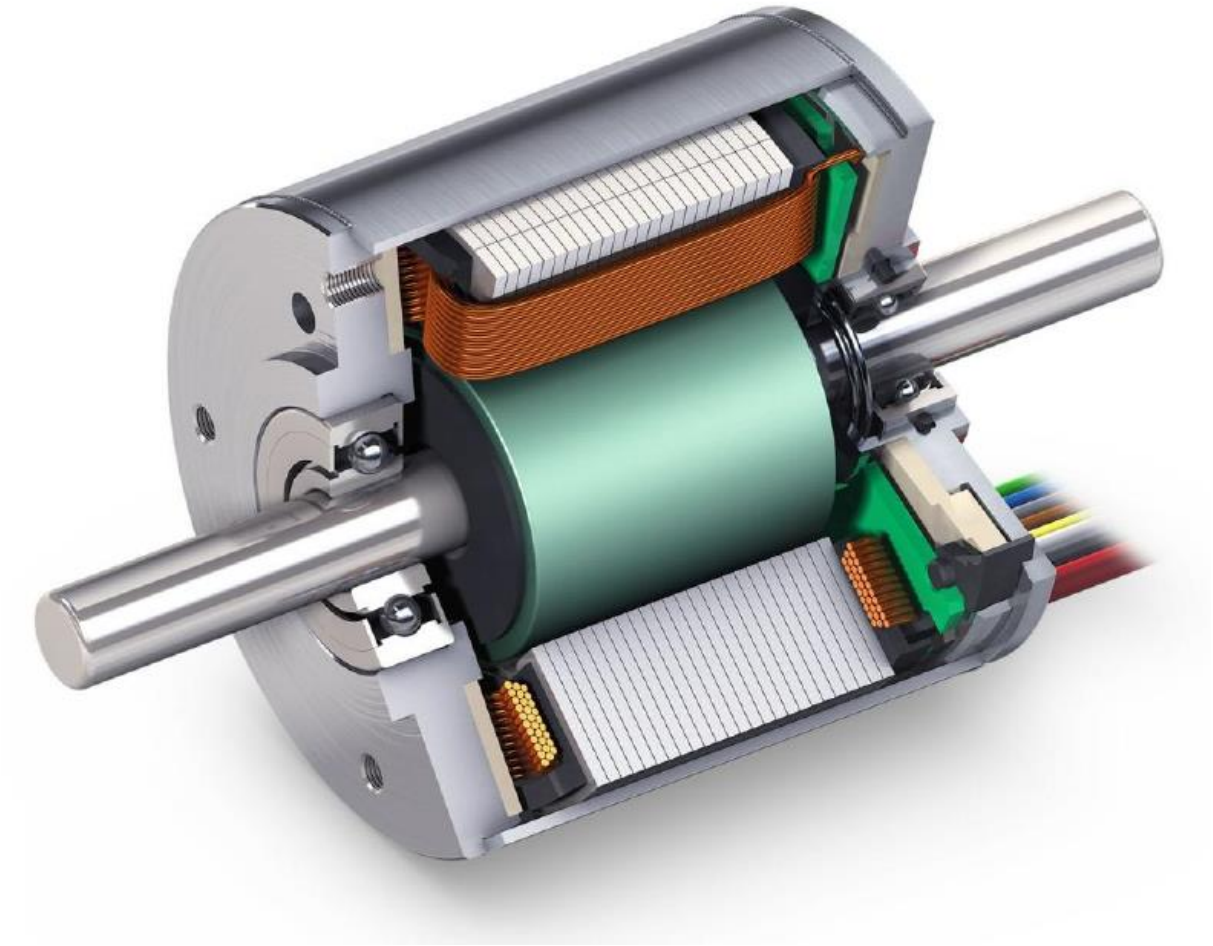

Figure 2.1 - Cross-section of BLDC motors

Brushless DC motors are the most used in the aerospace field, inside Electro-Mechanical Actuators. These motors are usually more specifically defined as permanent magnet synchronous motors with electronic commutation. They are formed by a stator case, usually in aluminium, that host the stator core on which the windings are coiled. The stator windings are connected with a three-star scheme. The differences from the brushed motors are: windings on the stator eliminate the need of brushes to mechanical perform the commutation between the phases, but introduces the need of electronic commutation, the elimination of brushes (typically made of graphite, a weary and conductive material) and particles that comes from brushes wear.

The brush commutator must be replaced by a solid-state electronic controller that regulates the “switching” sequence of the phases based on sensor measurement.

The most common design features three Hall sensors, possibly sharing the rotor permanent magnets, to determine the rotor position, while other systems rely on the measurement of counter electromotive force acting on the non-driven coils. The latter are known as sensor-less controllers and provide a simpler and cheaper solution for the power electronics, but they are only suitable to open loop applications since the counter EMF measurement is difficult at low angular velocities, so an irregular torque is delivered near the zero-velocity condition in which a servo-actuator is supposed to operate for most the time.

2.1 Stator

The stator of a brushless DC motor is an assembly made of laminated steel, to reduce eddy currents phenomena; on this core copper windings are placed and usually coated with a thermal insulating polymer. The windings can be arranged in a star, or Y connection, or a triangle scheme. When comparing motor characteristics, it’s useful to know based on which of the two schemes the electrical resistance is given.

The main difference is that in a delta connection phase voltage is equal to line voltage, while in a star connection phase voltage is equal to 1/ 3 of line voltage: so, when the same line voltage is applied, with the delta connection a higher current flows in the coils, thus delivering a higher torque compared to the same motor with a star connection. However, with delta connection a phase cannot be left unpowered and the commutation sequence is necessarily different: therefore, a star connection is generally employed unless special motors are used.

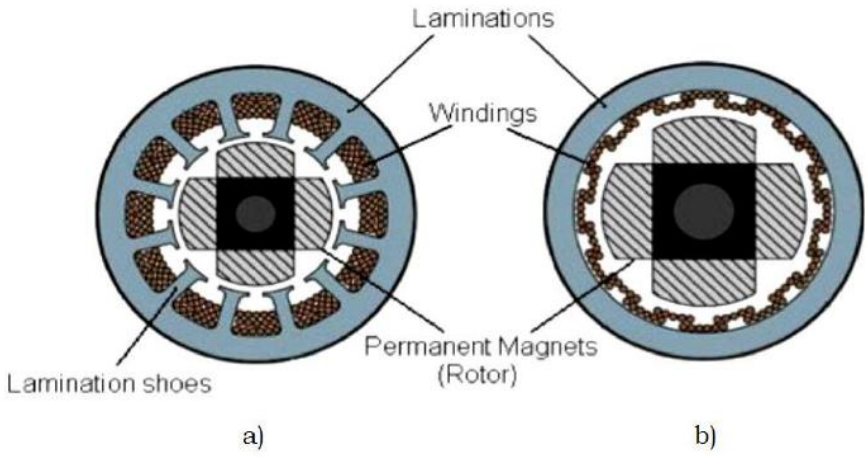

Figure 2.2 - Slotted (a) and slotless (b) stator

Steel laminations in the stator can be slotted or slot-less as shown in Figure 2.2. A slot-less core has lower inductance; thus, it can run at higher speeds since the phase commutation can be faster. Moreover, due to the absence of teeth in the lamination stack, cogging torques are reduced, thus making them an ideal fit for low speeds too. On the other hand, the greater air gap reduces the maximum available torque.

2.2. Rotor

In the rotor shaft of a BLDC motor the magnets are positioned. They are made from rare earth elements, like NdFeB that can generate a high magnetic flux (nearly over 1 Tesla) an is a good economic compromise, since the neodymium is the most common of the rare material. The magnetic flux influences both the motor Torque coefficient and the Back-EMF coefficient, so the use of this type of material highly enhance the performances. Depending on the application the number of magnets that are aligned on the stator may vary.

A higher number of magnets (i.e. an high number of magnetic poles) reduces the ripple of torque value, thus giving a “smoother” torque, but sets a maximum speed limit due to the limit of the switching frequency, in the control electronics, usually, two to eight pairs of poles are fit.

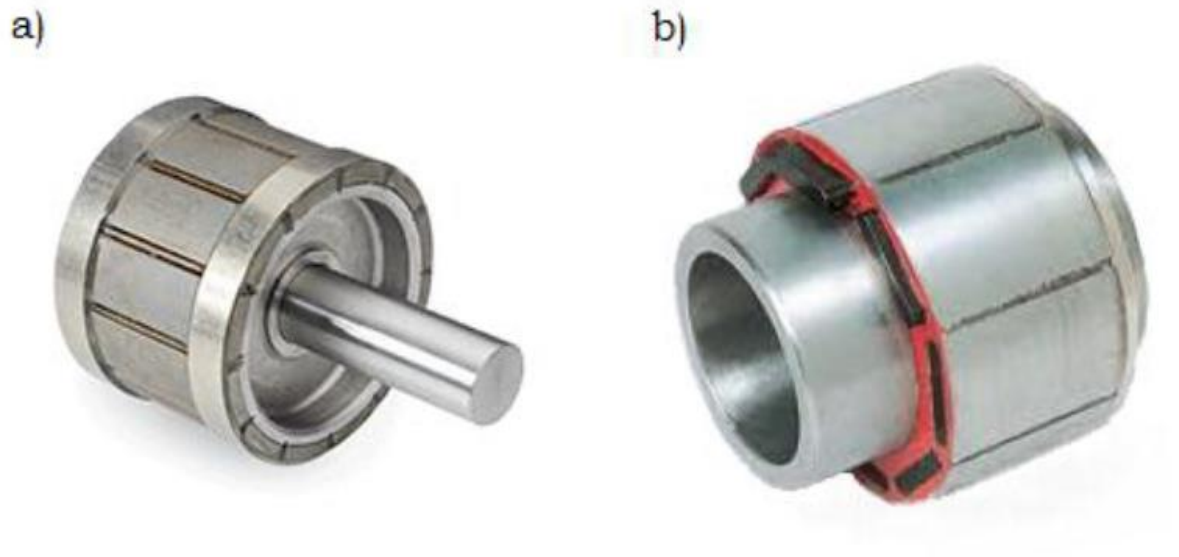

Figure 2.3 - Isotropic (a) and Anisotropic (b) rotors

2.3 Working Principles and Operation

The controller of a Brushless DC motor can use a square waveform (brushless Dc motor) or a sine waveform (brushless synchronous motor), to create currents and voltages to impose to the motor phases. It also depends on the shape of the counter electromotive force due to the distribution of magnetic flux density over the rotor.

Although AC brushless motor outputs a more regular torque, the most used are the brushless DC due to their manufacturing and control simplicity; the motor used in this work a DC Brushless type of motor.

The principle of operations for both BLDC motors and permanent magnets brushed motor is the same, since the first is often represented as a three-phase equivalent of the second. To control the position of the rotor the feedback from sensor is used to be fed to the commutation logic.

In brushed motors this is done mechanically via the brushes and commutator assembly, on the other hand, in BLDC motor there are no brushes and the windings are on stator and not on the rotating shaft. The commutation is then performed by a solid-state inverter circuit thanks to the measurements of a dedicated sensor. Usually, three (or multiple for redundancy reasons) Hal sensors are used and evenly spaced at 120° over the electrical revolution. This gives a measure of the position signal with a 60°degrees resolution. Note that the electrical angular position can be derived from the mechanical angular position, multiplying its value by the number of pole pairs of the motor.

The following example explains the concepts using a single pole pair motor for simplicity. Every 60° magnetic field in correspondence of one of the sensors reverses its polarity, and the signal is processed by the controller to determine which phases to power.

Figure 2.5 describes the commutation logic over one revolution; in Figure 2.5 (a), H1 and H3 sensors are located over the rotor south pole and generate a high signal, while H2 sensor sees the north pole and generates a low signal; then, phase A is unpowered, while phase B is connected to supply voltage and phase C is connected to ground.

Sixty degrees later, the north pole passes under the H1 sensor, which switches to a low signal (figure 2.65 (b)): as a result, phase C is deactivated and phase A is connected to ground, rotating the stator magnetic field by 60°. As shown in figure 2.5 (c), another sixty degrees later the H2 sensor switches to high output, phase B is turned off and phase C is connected to supply voltage: the stator field rotates another 60°. Then the commutation is continued in the other three figures to complete a revolution.

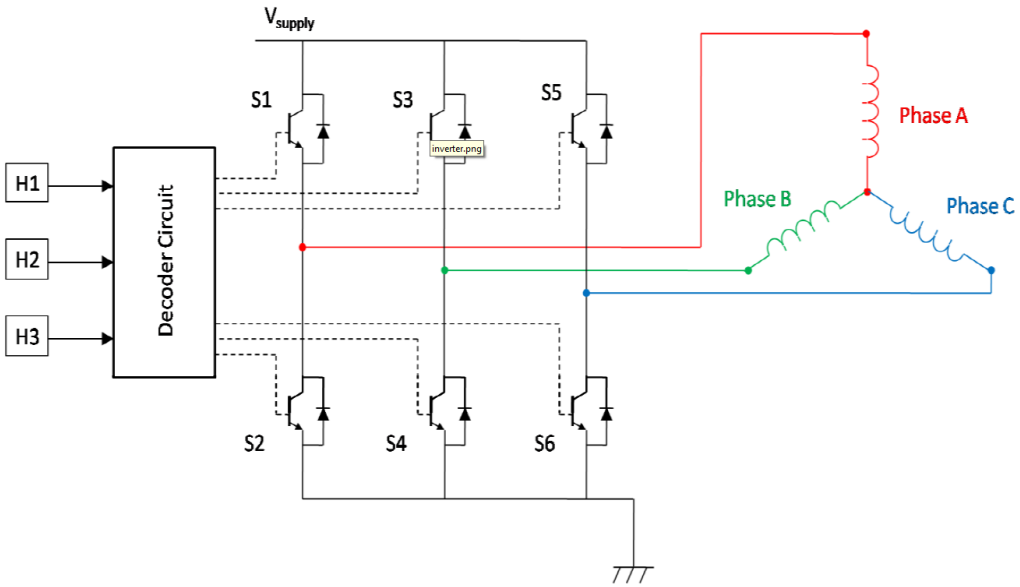

Figure 2.4 - Electrical scheme of the static inverter

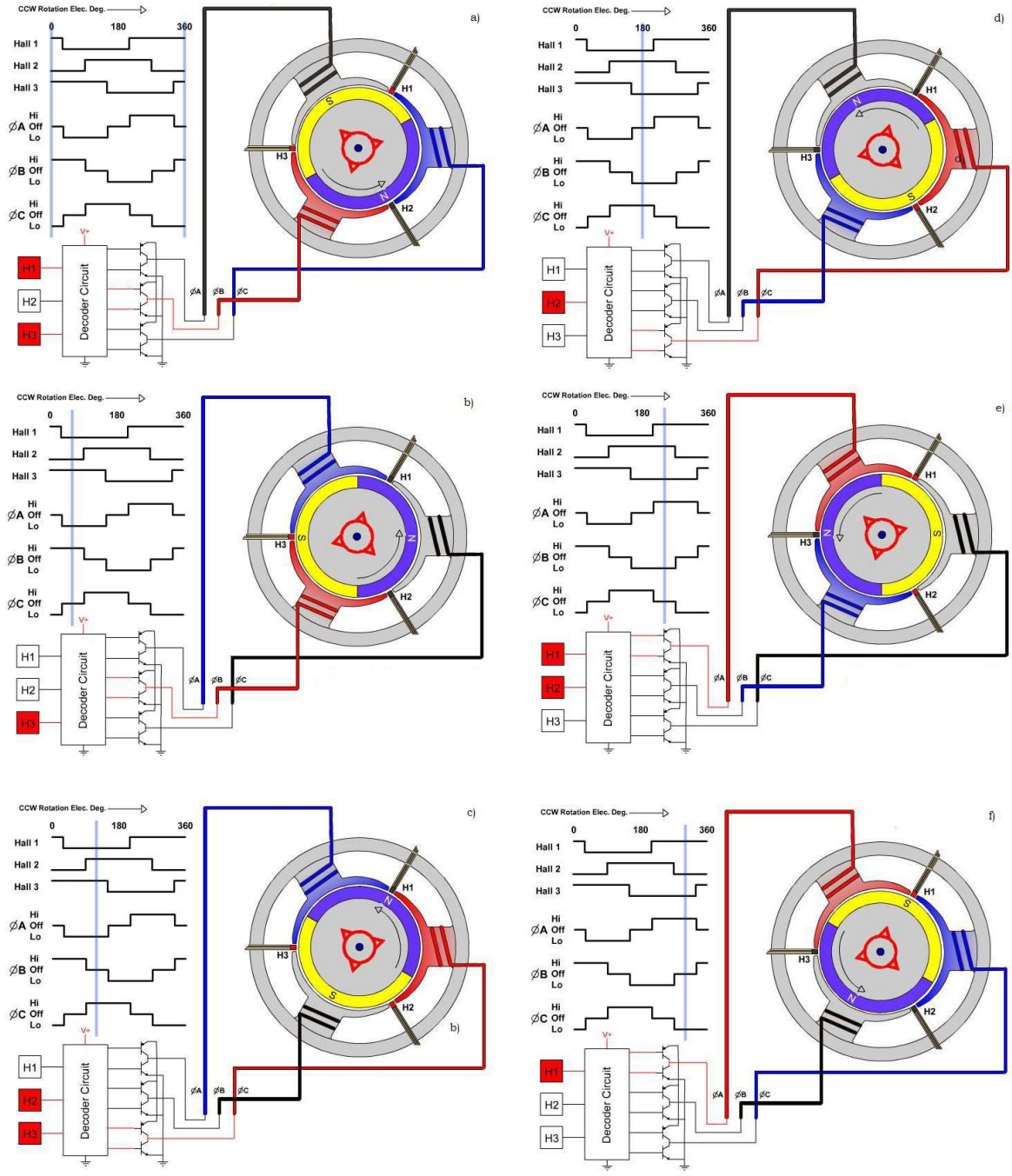

Figure 2.5 - Commutation sequence for a three phase, single pole pair BLDC motor

Electrical position		**$0 < \theta_e$** < 60°	**60° < θ_e** < 120°	**120° < θ_e** < 180°	**180° < θ_e** < 240°	**240° < θ_e** < 300°	**300° < θ_e** < 360°
Hall sensors	**H1**	1	0	0	0	1	1
	H2	0	0	1	1	1	0
	H3	1	1	1	0	0	0
MOS	**S1**	off	off	off	off	**on**	**on**
	S2	off	**on**	**on**	off	off	off
	S3	**on**	**on**	off	off	off	off
	S4	off	off	off	**on**	**on**	off
	S5	off	off	**on**	**on**	off	off
	S6	**on**	off	off	off	off	**on**
Motor Phases	**A**	off	**ground**	**ground**	off	**supply**	**supply**
	B	**supply**	**supply**	off	**ground**	**ground**	off
	C	**ground**	off	**supply**	**supply**	off	**ground**

Table 2.1- MOS switching sequence

Table 2.1 refers to Figure 2.5 and reports the complete switching sequence as a function of Hall sensors output. The phase activation is determined by a decoder logic circuit acting on the six power transistors of the inverter circuit which operate the commutation. It can be noticed that in every moment only two phases are powered: on the one hand, this allows cooling of the unpowered phase, on the other hand the motor maximum torque is reduced since only 2/3 of the coils are active at a time.

2.4 Torque and efficiency

Torque of a BLDC motor is generated by the interaction between rotor permanent magnets and stator windings. A stator coil is a magnetic dipole immersed in the magnetic field produced by the rotor; the dipole moment of the coil is, as a first approximation:

$$\boldsymbol{m} = NAi\boldsymbol{n}$$

where N is the number of windings in the coil, A is the area of the coil, i is the current and $\boldsymbol{n}$ is the normal versor to the coil plane. Torque exchanged between coil and rotor is then:

$$\boldsymbol{T}=\boldsymbol{m}\times\boldsymbol{B}$$

where $\boldsymbol{B}$ is the rotor magnetic field. In a more general notation, regardless of motor geometry, torque is proportional to current by a constant k_T. Total torque is then given by adding, in a vector sense, contributions by the three phases. As it can be noticed, torque is maximum when stator and rotor magnetic fields are perpendicular, so the commutation logic activates the phases to keep the stator field as close to normal as possible to the rotor field. Output torque of the motor can be increased by increasing current, number and area of windings, or the permanent magnets flux density; however, maximum current is limited by overheating problems due to Joule effect in the coils, and flux density of permanent magnets is limited by physical properties of known materials, among which Neodymium-Iron-Boron alloys show the best performance. Eventually, increasing area or number of windings results in a bigger and heavier motor.

Rotation of the motor causes the variation of magnetic flux crossing each coil which induces, according to Faraday's law, a counter electromotive force on the phases; this voltage is proportional to rotor angular velocity by the counter electromotive constant k_{BEMF}, which can easily prove to be $k_{BEMF}=k_T$. Therefore, current and torque are progressively reduced as speed increases; being:

$$V=Ri+k_T\omega$$

it results:

$$T = k_T i = Vk_T/R - \omega\, k^2{}_T/R\omega$$

and output power is:

$$P_{out} = T\omega = V\omega k_T/\mathrm{R} - k^2{}_T\omega^2/\mathrm{R}$$

whose trends are shown in Graph 2.1. It can be noticed from the graph that torque is maximum with the rotor stopped and decreases linearly with speed, while maximum power corresponds to half the maximum no-load angular velocity. Efficiency η is defined as the ratio between output power and input power:

$$\eta = \frac{\mathrm{Pout}}{\mathrm{Pin}}$$

being $P_{in} = V_i$, it results:

$$\eta = \frac{\mathrm{k_T}\omega}{V}$$

In the above derivation losses due to friction and viscous effects have been neglected, since they are usually small compared to Joule effect losses.

2.5 Motor Control

Several different control modes are available for BLDC motors, depending on the controlled variables and the purpose of the regulation.

A speed control mode can be employed for a system requiring a rate command, such as operating a hydraulic pump or a compressor, or as the inner loop of a position control mechanism like a servo-actuator. The phase commutation sequence is only related to rotor angular position measured by the Hall sensors, so it cannot be modified for a speed control purpose; angular velocity is indeed regulated by acting on amplitude of the applied voltage. Usually a constant voltage DC source is available, and the employ of a variable resistor leads to a low power efficiency of the system: in fact, the potentiometer controls voltage by dissipating excess power via Joule effect; a more efficient way of regulating the phase voltage is the implementation of a PWM logic, which applies high frequency pulses with a variable duty cycle:

then, the signal is filtered by the circuit inductance resulting in a voltage that is intermediate between supply and ground, proportionally to the PWM duty cycle.

The speed of the motor is calculated from signals of the Hall sensors and then compared to the required speed. The error is employed to vary, through a proportional or PID controller, the PWM duty cycle and eventually matching the motor velocity to the required speed.

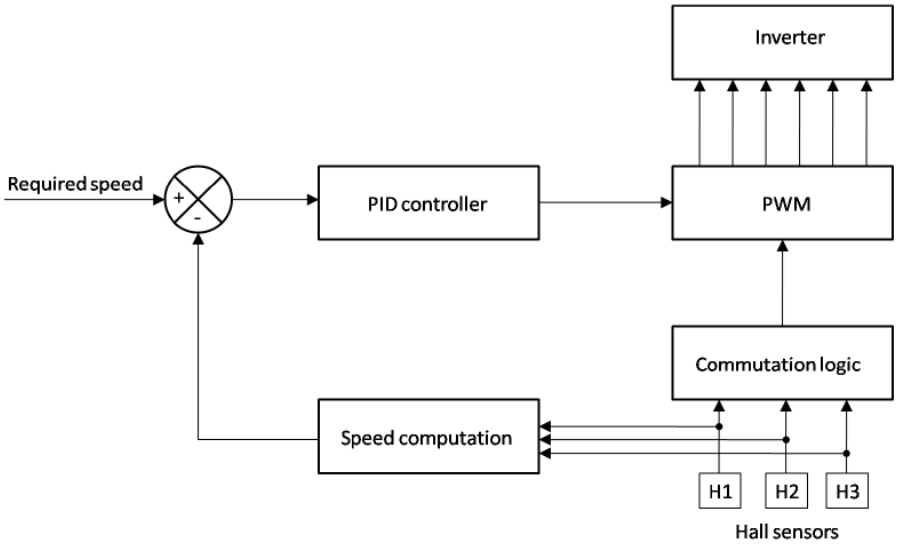

Figure 2.6 - Block diagram of a speed control loop

Some applications require instead a torque control mode, that means the motor is forced to deliver a constant torque regardless of speed and external load. This control mode can be useful for operation of some industrial equipment or, once again, as the inner loop of a position control system. Torque delivered by the motor depends on magnetic flux distribution through the phase coils, which in general requires complex and computationally expensive electromagnetic FEM simulations; however, it has been shown how torque is proportional to phase currents by a constant k_T, which is one of the most important motor specifications. Therefore, torque con be controlled by acting on the phase currents: a total current can be computed by measuring the voltage drop due to the ground line resistance and the resulting value,

multiplied by k_T is compared to the required torque command signal. The torque error is then fed to a PID controller which modifies the PWM duty cycle in a way like the speed control mode, regulating phase voltages and consequently phase currents. Hence, the only difference between torque and speed control mode stands in the measured variable.

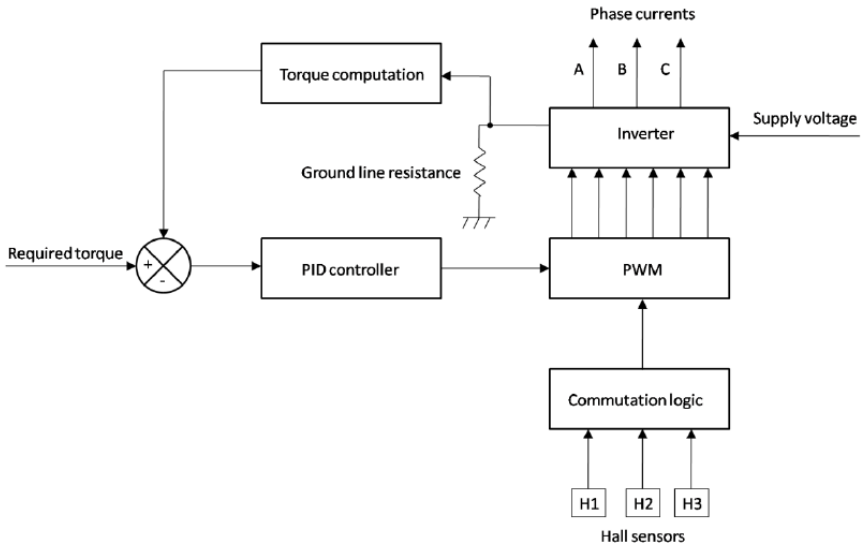

Figure 2.7 - Block diagram of a torque control loop

Some operating conditions can cause irreversible damages to the motor: for example, when a high external load causes the rotor to get stuck, counter electromotive force drops and phase currents grow to a very high level, causing overheating and possibly damaging the coil insulation, demagnetizing rotor permanent magnets (it has to be noticed that NdFeB high performance magnets have a very low Curie point and can be safely operated at temperatures not higher than 80 ℃), or burning the power electronics; a sudden velocity reversal can induce a high stator magnetic field and demagnetize the rotor. In these cases, to prevent a failure, a *motor protection* control mode overrides the normal control to preserve the system.

Peak current is the maximum current allowed in fast transients such as at starting from a motionless condition; whenever this value is crossed, a motor protection logic cuts the PWM output. *Maximum working current* is the maximum value allowed during normal operations; a firmware logic

automatically reduces the PWM output if this limit is exceeded. Other protection modes are the undervoltage protection, used when the system is battery operated to avoid damaging a lithium polymer battery, or identification of a faulty Hall sensor: this occurrence prevents the commutation to operate the motor smoothly and safely, so it results in a power cut-off. Recognition of a faulty Hall sensor is quite easy, since only some combination of their outputs are allowed by the motor geometry: only one sensor can change its output at a time and the three sensors are not allowed to generate the same signal; if a sensor is not working correctly, a non-allowed pattern will be recognized by the control logic. However, this fault isolation is not useful for prognostics purposes, as such damage is usually sudden and leads to a total system failure, and therefore it is not considered in this work.

2.6 Faulhaber Brushless DC-Servomotor 4490 B

Different BLDC motors where examined during the initial phase of this work

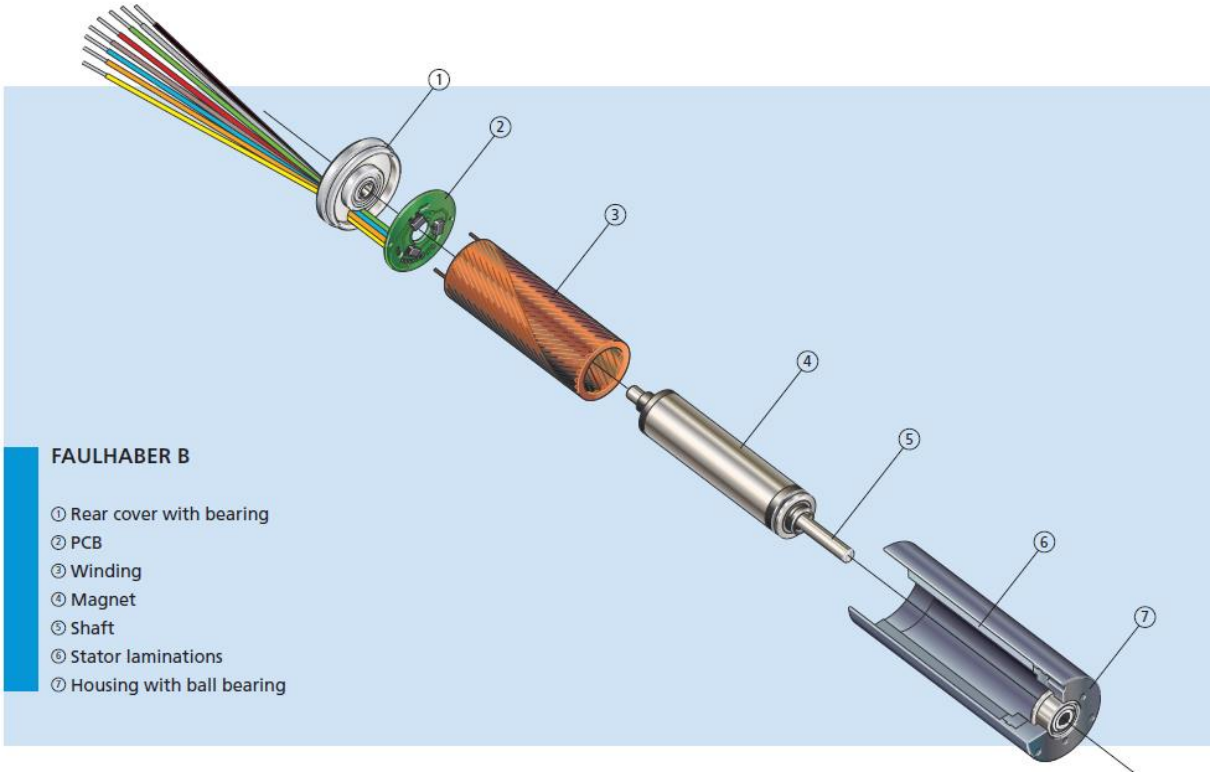

Figure 2.8 - Faulhaber DC-Motor (B-type) [4]

and Faulhaber Brushless DC-Servomotor model 4490 B and 4490 BS were chosen (48 V supply). Although all the models and simulation that follow from this point on will only report results relative to 4490 B. Faulhaber motor has a peculiar type of stator called “coreless” (or ironless. This system consists in a self-supporting, progressive, skew-wound rotor applied to a three-phase brushless DC-motor with a slotless rotor.

The benefits of this type of technology includes [4]:

- No cogging torque resulting in smooth positioning and speed control and higher overall efficiency than other brushless motor types;
- High torque and high performance in relation to the size and weight of the motor;

- Linear relationship between load to speed, current to torque, and voltage to speed, with a highly sensitive current torque behavior;
- Extremely low torque ripple.

In Table 2.2, will be given a brief description of the motor main characteristics and a short explanation of the ones involved with thermal simulation.

- *Slope of n-T curve*, $\Delta n/\Delta T$: the ratio of the speed variation to the torque variation. The smaller the value, the more powerful the motor;

$$\frac{\Delta n}{\Delta T} = \frac{R}{{k_M}^2} \cdot \frac{1}{2\pi}$$

- *Current constant*, k_I: the ratio of variation of the current depending on the output torque, also the reciprocal of the torque constant k_M;
- *Terminal inductance*, L: measured between two phases at 1 kHz;
- *Mechanical time constant,* τ_m: the time it takes the motor to reach 63% of the final value with no-load, from 0 rpm;

$$\tau_m = \frac{R\,J}{{k_M}^2}$$

- *Angular acceleration*, α_{max}: acceleration under no load condition from standstill;

$$\alpha_{max} = \frac{T_0}{J}$$

Series 4490 ... B [@ 22°C and nominal voltage]				
Characteritic		Symbol	Value	Measurement Unit
Nominal Voltage		U_N	48	V
Resistance phase-phase		R	0,7	Ω
Inductance phase-phase		L	235	μH
Efficiency MAX		η_{MAX}	87	%
No-load speed		n_0	10 800	rpm
No-load current		I_0	0,317	A
Stall torque		T_S	2,978	Nm
Friction Torque, static		T_{0S}	$4{,}96 \cdot 10^{-3}$	Nm
Friction Torque, dynamic		T_{0D}	$7{,}72 \cdot 10^{-1}$	Nm/rpm
Speed constant		k_N	220	rpm/V
Back-EMF constant		k_E	$4{,}56 \cdot 10^{-3}$	V/rpm
Torque constant		k_M	$4{,}35 \cdot 10^{-3}$	Nm/A
Current constant		k_I	23	A/Nm
Slope of n/T curve		Δn/ΔT	3,5	rpm/Nm
Mechanical time constant		τ_m	4,8	ms
Rotor Inertia		J	130	gcm^2
Angular acceleration		α_{max}	$229 \cdot 10^{-3}$	rad/s^2
Thermal resistance		R_{th1} / R_{th2}	0,96 / 3,9 (5,2)	K/W
Thermal time constant		τ_{w1} / τ_{w2}	23 / 1222	s
Operating temparature range				
	motor	from -30 to +125		°C
	winding, max	to +125		°C
Mass		m	0,742	kg
Angular speed, max.		n_{max}	18 000	rpm
Housing material		Aluminium		
Magnet material		NdFeB		
Rated values for continuous operation				
Rated Torque		T_N	0,137 (0,19)	Nm
Rated Current		I_N	3,91 (4,37)	A
Rated Speed		n_N	10 930	rpm

Table 2.2 – Motor datasheet

- *Thermal resistance,* R_{th1}, R_{th2}: [4] "R_{th1} corresponds to the thermal resistance between the windings and the housing. R_{th2} corresponds to the thermal resistance between the housing and the ambient air. R_{th2} can be reduced by enabling the exchange of heat between the motor and the ambient air (for example, a thermally coupled mounting configuration, using a heat sink and/or forced air cooling). This will be examined in Chapter 4 about thermal modelling. R_{th2} has a double value since 3,9 K/W is a reduction by 25% of the real value with conventional method of installation (5,2 K/W for mounting on a metal flange);

- *Thermal time constant,* τ_{w1}, τ_{w2}: these two are relative to the time it takes to windings and housing to reach 63% of the steady state temperature;

- *Maximum speed,* n_{max}: this value is determined considering the service life of the motor. Exceeding this recommended value will reduce the useful life;

- *Rated Torque,* T_N*:* the maximum torque at S1 type of operations, meaning that steady state temperature is reached, but not exceeded. In this condition the motor can run continuously without stopping and remaining in the operating temperature range and not exceeding the maximum winding temperature. The motor can provide a higher torque in S2 or S3 (intermittent) operations or if more cooling is added (in the BLDC model a natural convection cooling is assumed, see Chapter 4);

- *Rated Current* I_N: the meaning of nominal I similar the one referred to the torque. This value keeps in consideration the effects of a loss of k_M (torque constant) as it relates to the temperature coefficient of the winding, losses due to effects of the dynamic coefficient of friction which include the Foucault (eddy current) losses, as well as the thermal characteristics of the given magnet material. As per the nominal torque, this value can be exceeded only in case of non-continuous

operations and/or if an active cooling system is use (fluid or servo-actuated fan);

- *Rated Speed* n_N: The typical speed at steady state resulting from the application of the given rated torque. This value includes the effects of motor losses on the slope of the n/T curve;
- *Rated slope of the n/T curve*: An approximation of the slope of the curve at a given rated operating point. This value is derived from the no load speed and the speed a under load.

$$\frac{n_0 - n_N}{T_N}$$

3. Electromechanical actuator modeling

A model is a mathematical representation of a system, based on physical principles. The advantages of having a model instead or in addition to the system that is object of the analysis may be many, but two major benefits (compared to pure experimental methods) are:

- The model is useful if the physical system is inaccessible. This might be for economic reasons, if the system is still under development, if the analysis is too dangerous for real experiments or even if the analysis, like in prognostic field, is expected to damage the physical system (e.g. testing of prognostic algorithms that has to evaluate a possible phase short circuit);
- The model can "extrapolate" the system behavior: this meaning that simulation data obtained is transparent to the operating conditions in which the physical system is operating;

The model of the Electro-Mechanical Actuator has a high level of detail and it represent a highly nonlinear dynamic. The model is derived from Maggiore, Dalla Vedova and Berri works [5]. Being the field of the research the Prognostic of EMAs, all blocks representing EMAs fault has not being removed and can be object of future works in failure identification algorithms.

The model is developed using Simulink software and Simscape environment is used to model the electrical and the thermal networks. The latter enables the creation of models of physical systems as groups of "networks" of different physical domain. The difference between Simscape and Simulink in this context is that the first gives a "realistic" and more intuitive overall vision of the modeled system as the connection between block are proper physical dimensions. Also, it uses some blocks that allows the integration of networks from different physical domains.

The goal of having such a model available is to make it real-time viable, so that it can be possible to run it during pre-flight operations or even in flight. To make this possible it's necessary find out if the simulation performance meets the requirements to avoid overrun when the model is simulated on a real-time processor. Although there are different methods to preliminarily estimate performance of a simulation, this kind of work goes beyond the purpose of this thesis, so their implementation might be useful for future works.

Due to the complexity of the model and to the variety of the physical domains, with differently time-varying parameters, the simulation is computationally quite expensive, since it takes almost 15 minutes to simulate 10 s of operations of the EMA. The simulation time can also increase depending on the Load conditions: if there is no load applied to the external surface, the total simulation time is reduced.

Also, the model is moderately stiff, and it requires a variable-step solver like *ode23t* (for moderate stiffness problem, using Trapezoidal rule*)* with a relative tolerance of *1e-4* to be simulated within a reasonable amount of time. In Simscape is very usual to have moderately to highly stiff models since they often have multi-physical networks and therefore, they have both fast varying and slow varying dynamics (in addiction to multiple zero-crossing, which further increase the simulation time). Note that MATLAB has many different ode solvers to compute the solutions to systems of ODEs (Ordinary Differential Equations) and/or DAEs (Differential and Algebraic Equtions). The choice is between those solvers that can handle moderately stiff problems and DAEs (Differential Algebraic Equation systems), with the same convergence rate both for differential and algebraic variables. MATLAB has four solvers to use in case of stiff problems: ode15s, ode23s, ode23t, ode23tb, where the digits in the name are relative to the order of the underlying algorithm, the letter "s" stand for "stiff" and "t" and "tb" are relative to two variations of the trapezoid method used in the ode functions [10].

For the simulation of important kinds of electrical circuits ode23t is suited among the different alternatives [11].

Simulation Parameters			
Variable Name	Description	Value	Measurement Unit
simulation.TiBr	Simulation duration	10	s
simulation.DT	Integration step	$1 \cdot 10^{-6}$	s
simulation.tauFilter	Characteristic time filter I_3eq	$5 \cdot 10^{-5}$	s
controller.Gprop	Proporzional gain controller	$1 \cdot 10^{-5}$	1/s
controller.W_refMax	Speed saturation	18 000	rpm
controller.I_Max	I_ref Saturation	34,25	A
controller.Knoise	Noise Coefficient	0	-
controller.PID.GAP	Poportional Gain PID	0,05	Nm s /rad
controller.PID.GAI	Integrative Gain PID	0	Nm / rad
controller.PID.GAD	Derivative Gain PID	0	Nm s /rad
controller.PID.ErIM	Max Integrator error	100	Nm
inverter.PWM.hb	Hysteresis band	0,2	A
inverter.Hbridge.Vdc	Supply Voltage	48	V
inverter.Hbridge.RSnubber	Snubber Resistance	$1 \cdot 10^{-5}$	Ω
inverter.Hbridge.CSnubber	Snubber Capacity	inf	F
inverter.Hbridge.Ron	Ron (in Universal Bridge)	$1 \cdot 10^{-2}$	Ω
BLDC.P	Pole Pair	2	-
BLDC.Nabc	Fraction of active windings (A, B, C) - non faulty conditions	[1 1 1]	-
BLDC.Rs	Nominal resistance phase-phase	0,7	Ω
BLDC.Ls	Nominal inductance phase-phase	$2{,}35 \cdot 10^{-4}$	H
BLDC.Ke	Torque constant	0.0435	Nm/A
BLDC.TMM	Torque saturaton	2,978	Nm/A
BLDC.zeta	Rotor static eccentricity module - non faulty conditions	0	-
BLDC.phi	Rotor static eccentricity phase - non faulty conditions	0	-
dynamics.tau	Gear ratio	1/500	-
dynamics.JM	Motor Inertia	1,3 · 10-5	kg m^2
dynamics.CM	Viscous friction coefficient - Motor	$9{,}4248 \cdot 10^{-5}$	N m s/rad
dynamics.JU	User Inertia (slow shaft) reduced to Motor shaft	$1{,}2 \cdot 10^{-5}$	kg m^2
dynamics.CU	Viscous friction coefficient - User	$4{,}507 \cdot 10^{-7}$	N m s/rad
dynamics.friction.FSTm	Static friction motor	0,06	
dynamics.friction.FDTm	Dynamic friction motor	0,03	
dynamics.friction.FSTu	Static friction user	0,04	
dynamics.friction.FDTu	Dynamic friction user	0,02	

dynamics.BLK	Backlash width	$5 \cdot 10^{-5}$	rad
dynamics.ThUmin	Upper End-Stroke	1	rad
dynamics.ThUmin	Lower End-Stroke	-1	rad
therm.Te	External Temperature	295	K
therm.T0	Initial motor temperature	295	K
therm.mass.w	Windings mass	0,02	kg
therm.mass.sc	Stator Case mass	0,223	kg
therm.Rth1	Thermal resistance windings/stator case	0,96	K/W
therm.Rth2	Thermal resistance stator case/air	5,3	K/W
therm.Cp.w	Specific Heat (copper/windings)	450	J/(kg K)
therm.Cp.sc	Specific Heat (aluminum/stator case)	897	J/(kg K)

Table 3.1 – Simulation parameters

3.1 Simulink-Simscape Model

As shown in Figure 3.1 the model is composed of a Command Block, Test Load Block, Display Results Block and the EMA Block.

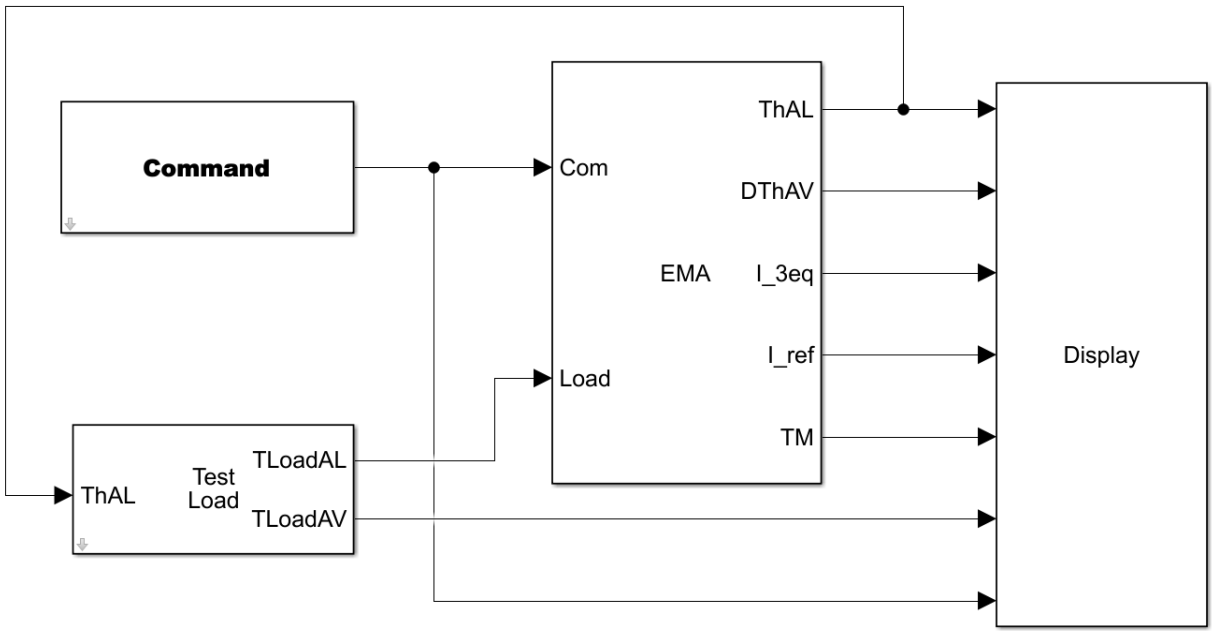

Figure 3.1 – EMA Simulink Block

3.1.1 *Command* Block

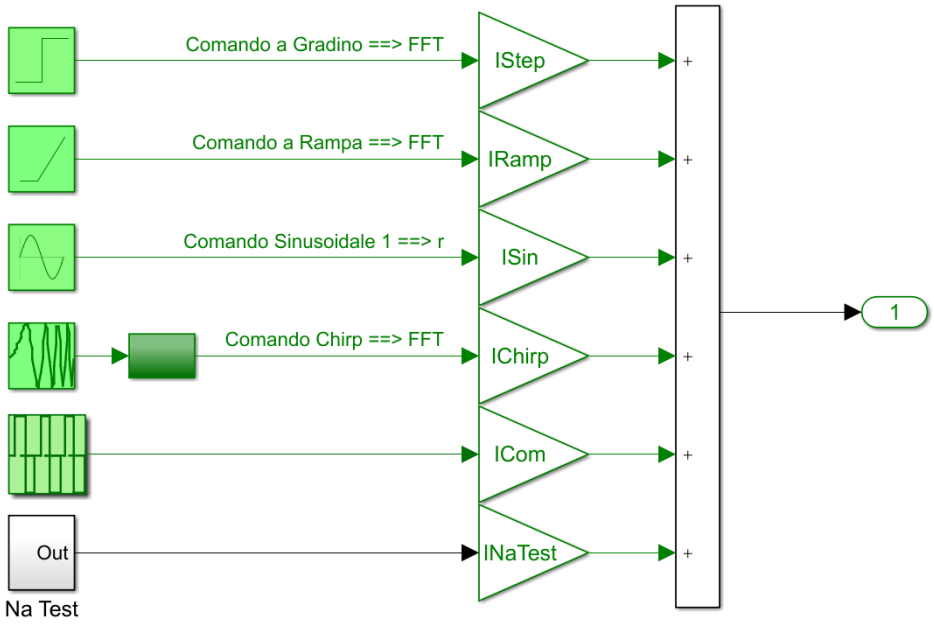

Figure 3.2 – Command Block

This block modulates the input signal (simulating a command by Flight Control System), chosen between different types of command, based on the type of analysis that is required. It is also possible to study a composite command based on the composition on two or more simple commands. The Command can be select directly from Mask Interface windows.

- *Step* [rad]. Defined by three parameters: Initial Amplitude, Final Amplitude and Instant of application;
- *Ramp.* Defined by: Time of application, ramp slope and Initial ramp output;
- *Sine wave*. Defined by: Frequency, Bias Input and Sem-amplitude input.
- *Chirp*. Defined by: Initial Amplitude, Initial Frequency, Target Frequency, Time instant at which Frequency Amplitude is reached;

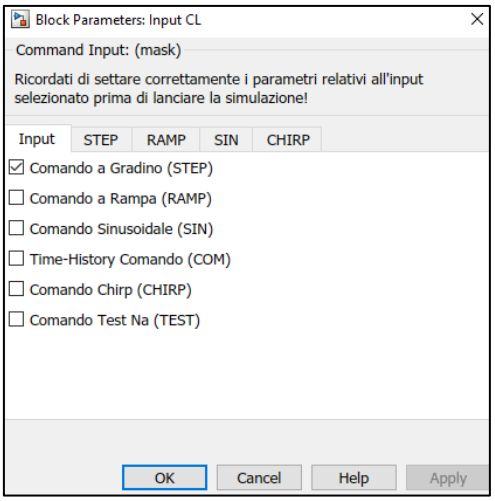

Figure 3.3 – Parameters for Command Block

- "User defined time history": from the data file .m the user can load a specific command history, to simulate a real flight scenario command sequence or to analyse it afterward.

Different commands can also be mixed and fed forward to the rest of the model. Command defining parameters can be defined directly in this block or in the input .m file data.

3.1.2 *Test Load* Block

In this block it possible to switch from three different type of Load condition on the actuator.

1. *No Load*: this option allows the analysis of the response of the EMA in an ideal no-load condition (therefore assuming a statically balanced surface) with 0 Nm opposing torque;

2. *Aileron/Primary Flight Surface*: assuming a Primary-like type surface the motor Stall Torque can be used to have a reference for the maximum Load Torque imposing a safety factor of 2 (100% more). Note that this is a "maximum load" on the surface, corresponding to a surface maximum deflection (end-stroke of the actuator). To simulate

a more real behaviour there is the need to have information about flight condition and surface geometry in order to have a Load proportional to the surface deflection;

$$T_{maxP} = \frac{T_0}{2} = \frac{2{,}978\ Nm}{2} = 1{,}489\ Nm$$

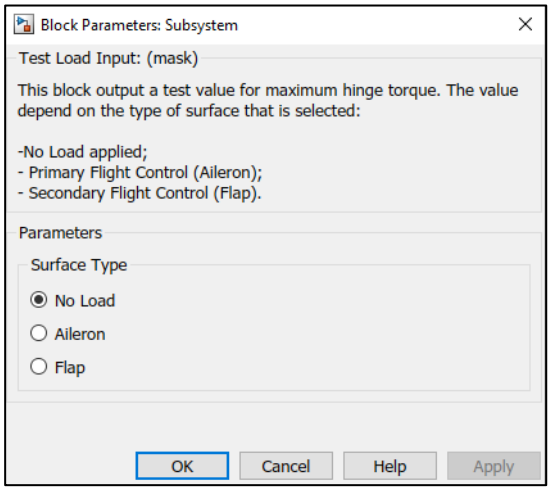

Figure 3.4 – Parameters for Load Block

3. *Flap/Secondary Flight Surface*: the same procedure is applied for the Secondary-like type of surface, with a safety factor of 1,5 (50% more of the maximum Torque).

$$T_{maxS} = \frac{T_0}{1{,}5} = \frac{2{,}978\ Nm}{1{,}5} = 1{,}985\ Nm$$

The safety factor is generally higher on Primary Surface since the maximum available net torque – difference between the motor and load torques - drives the actual actuation speed. Note that all the torque load is applied on the slow shaft, after the reduction is applied, but are scaled based upon the motor stall Torque T_0.

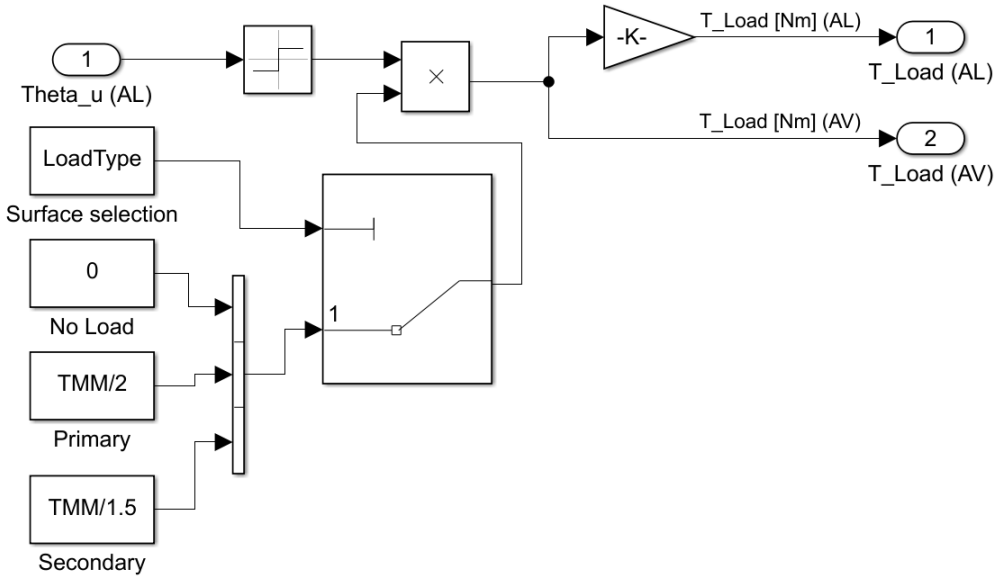

Figure 3.5 – Torque load block

3.1.3 *EMA - Control Electronics (PID)* block

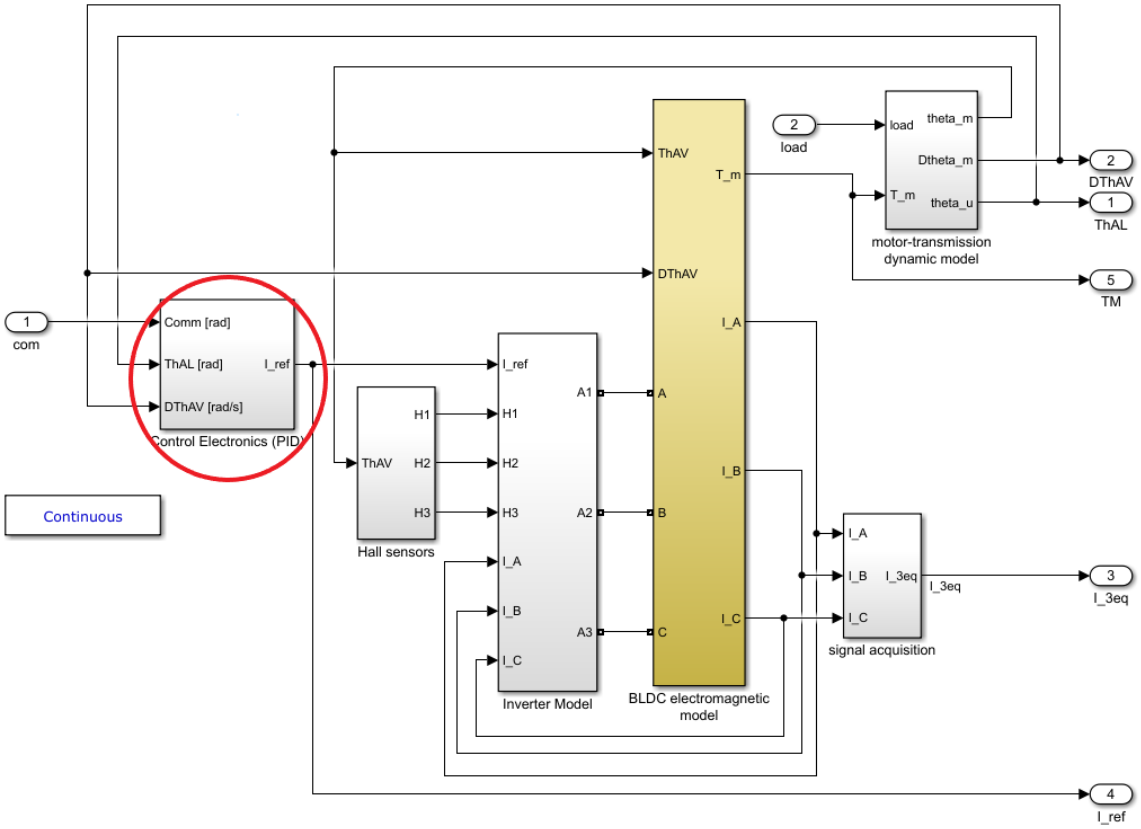

Figure 3.6 – EMA Block

In the *Control Electronics (PID)* block the command (`Comm`) signal is compared to the Slow shaft position (`ThAL`) and the resultant error (`Err_Pos`) is then proportionally controlled (G_{prop}) and saturated with `W_refMax` to be again compared to `DThAV` (Fast Shaft speed) to obtain an angular speed error (`Err_W`). Note that the saturation on the speed is applied to avoid overspeed that may damage the motor or reduce the Remaining Useful Life of the system.

The angular speed error is fed to a PID controller (`GAP, GAI, GAD`) which outputs a motor torque reference value (`TM_ref`), that, divided by motor torque constant gives the control current reference value. Note that this value is a control signal and not a physical current, since it doesn't represent the real current circulating in the three-phase motor but is used to perform phase commutation. The reference current is then saturated with a current value

that depend on thermal limit of the BLDC motor. The saturation current is based on the instantaneous maximum torque with a primary-like surface load condition (34,25 A), scaled with K_I.

The Derivative gain of the Control Loop is set to zero to avoid amplification of the white noise applied to the feedback signal; integrative gain is also set to zero, since the controller meets the requirements with a simple proportional logic. Ultimately a white noise disturbance is added to `I_ref` to simulate the noise affecting low power data transmission.

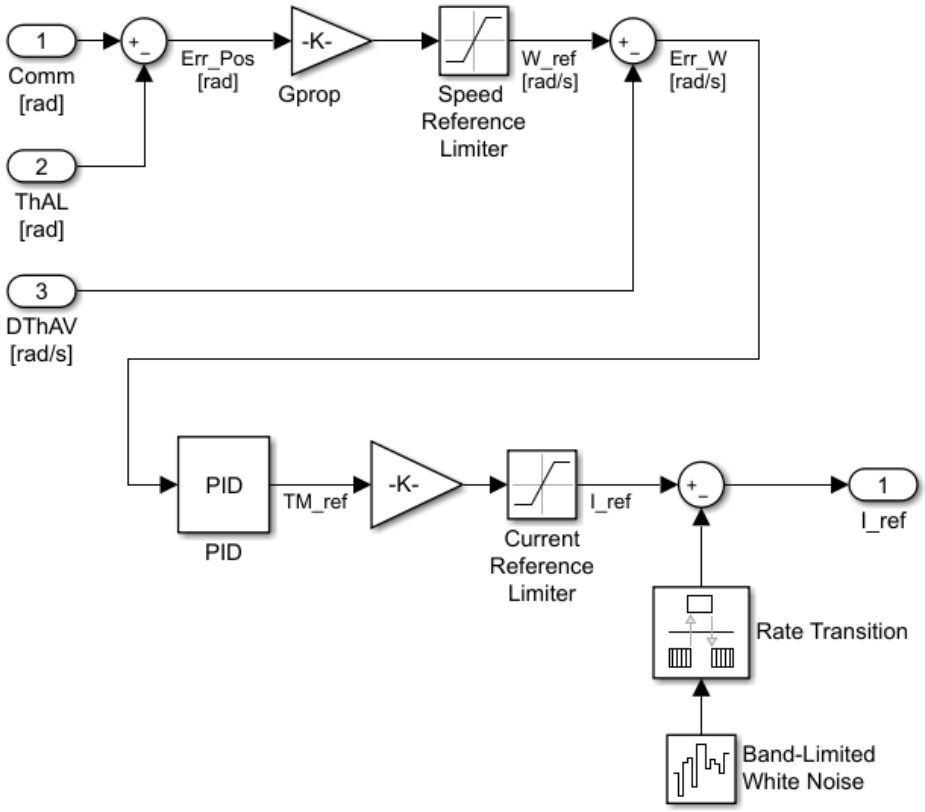

Figure 3.7 – Control logic block

3.1.4 *Hall Sensors* block – Active phase evaluation

In this block the electric angle is calculated (based on mechanical angle feedback from motor-transmission dynamical model) and the 3 signals, corresponding to the reading of the three hall sensors, are produced. This is

used to give the Inverter block information on the timing for switching on and off motor phases. The electric angle is:

$$\mathrm{Th_{el}} = 2\,\pi\left(\frac{\mathrm{BLDC.P}\ \cdot \mathrm{ThAV}}{2\,\pi} - \mathrm{floor}\left(\frac{\mathrm{BLDC.P}\ \cdot \mathrm{ThAV}}{2\,\pi}\right)\right)$$

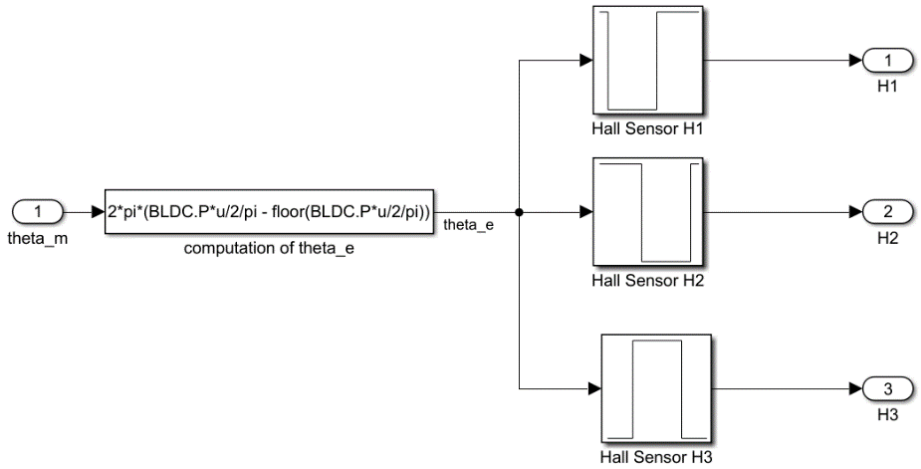

Figure 3.8 – Hall sensors block

3.1.5 *Inverter Model* Block

In this complex block it is shown the model of the static power electronic:

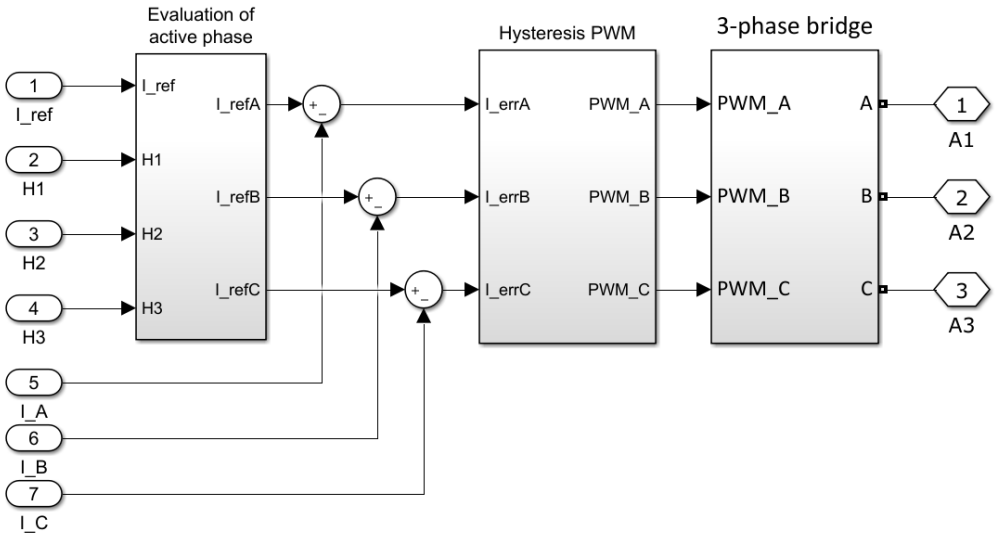

Figure 3.9 – Inverter model block

- *Evaluation of active Phase*: this block takes as input the `I_ref` signal coming from the control electronic and splits it into three different control current signals (`I_refA`, `I_refB`, `I_refC`) based on the position of the rotor i.e. the Hall sensors outputs (`H1`, `H2`, `H3`);

- *Hysteresis PWM*: in this block the three-phase current are compared to the current control signals to determine if the specific phase needs or not to be controlled. The error (difference between the `I_ref` and the actual I signal) is then fed to three corresponding hysteresis blocks to generate the PWM signals. The hysteresis output a 1 if the error signal is bigger than `+hb` (half of the dead band), -1 if the error is less `-hb` and 0 if the error lays in the block dead band. The dead band determines the PWM carrier frequency. For the Theorem of Nyquist-Shannon, this frequency needs to be one order of magnitude bigger than the inverter switching frequency to avoid aliasing problems.

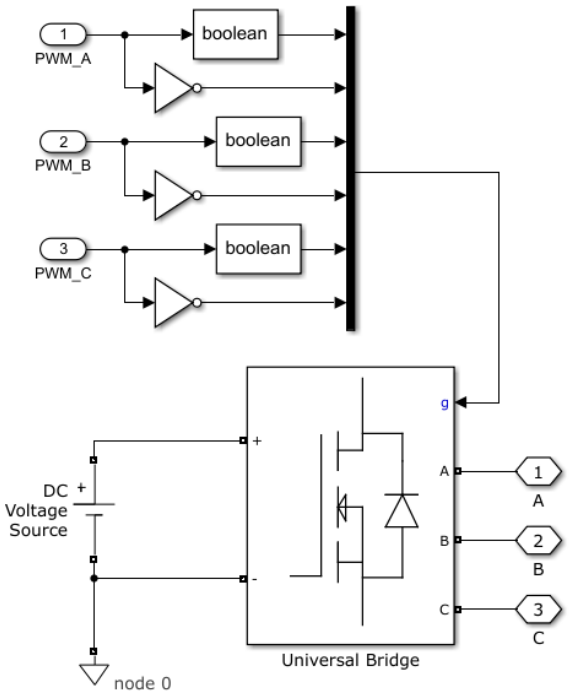

Figure 3.10 – Three Phase H-Bridge

- *3-Phase H-Bridge*: this block is made from the Simulink Specialized power System Library and the Universal Bridge Block equipped with

MOSFET / Diodes device. The bridge is supplied with a 48 V DC ideal voltage source and with 'g' 6 x 1 vector to control the switching of the MOSFET power transistor on the bridge. Every MOSFET has an assigned value in the vector: 0 the transistor is OFF; 1 the transistor is ON. The 'g' vector is composed from 3 signal so that on the same phase the two transistors have complementary switching, in order to avoid short-circuits between supply and ground inside the H-Bridge. The choice to use the H-Bridge block is for future prognostic reasons: with this block it will be possible in future works to include some more faults that involve the static inverter.

3.1.6 BLDC Electro-magnetic Model

In this block the BLDC electrical / thermal branch is modelled. The Thermal model block will be shown in detail in the next chapter.

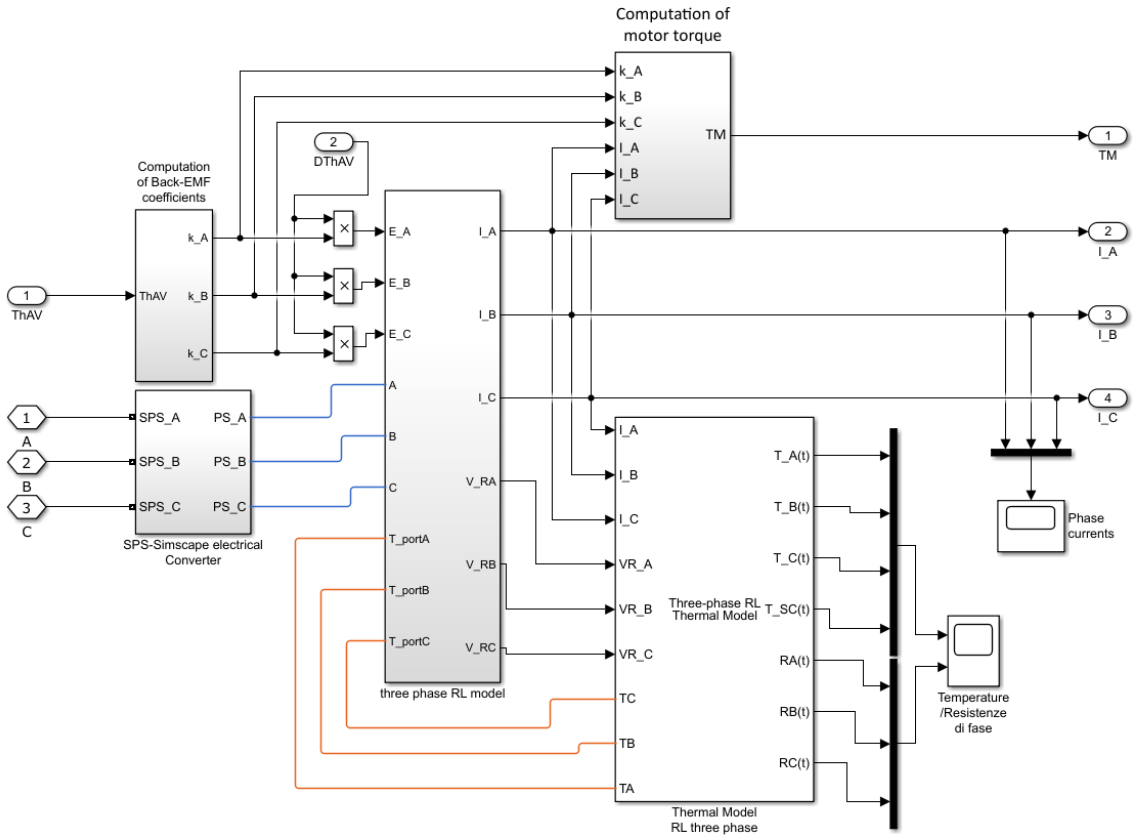

Figure 3.11 – Electro-magnetic model block

1. *Computation of Back-EMF* Block*:* The Back-EMF is calculated by multiplying the Back-EMF coefficient by the rotor angular speed (`DThAV`). This value is then passed to the BLDC electrical branch to evaluate the phase currents. In this block the electrical angle is derived and then a trapezoidal back-EMF constant is generated to be fed to a 3-blocks, that introduce the Static eccentricity fault. The ζ represents the static rotor eccentricity module; in non-faulty conditions its value is 0. Note that normalized counter electro motive force is equivalent to the electromagnetic coupling constant:

$$BEMF_{norm} = \frac{BEMF_{norm}}{DTh_m} = K_{fcem}$$

For this reason, it is used also to calculate the motor Torque in the *Motor torque computation* block. If the number of pole pairs of the BLDC rotor is major than one, the effect of rotor eccentricity is considered to fix electromagnetic coupling constant value as a function of rotor position Th_m:

$$k^i_{BEMF} = k^i_e(Th_m)\left(1 + \zeta cos\left(\dot{Th_m} + \frac{(\imath - 1)2}{3}\pi\right)\right)$$

Where $k^i_{BEMF}(Th_m)$ is the trapezoidal wave-shaped normalized back EMF force of the i-th phase of the non-faulty motor, evaluated by a look up table, and ζ is the ratio between rotor eccentricity and nominal air gap.

In this block it is also model the short-circuit fault, since an overcurrent in the motor coil windings can cause a damage on the electrical insulation of the single phase resulting in a possible short circuit fault. When a damage to the insulation is propagating, resistance and inductance values keep on increase and so does the current that is running in that motor phase. Therefore, the Power losses to the Joule effect increases as well, feeding the damaging process and propagating the damage to the whole phase winding.

There can be different type of short circuits:

- On the same phase between winding (coil-coil);
- Between two or more different phases (phase-phase);
- Between a phase winding and the iron stator core (phase-ground).

As already been said, a coil-coil short circuits cause the resistance and the inductance to decrease and an overall visible "asymmetry" in phase currents in the Simulink scope. The torque gain and Back-EMF are reduced too. The latter can be approximated to:

$$k_{BEMF} = G_M = \frac{\partial \Phi}{\partial \theta_m} = \mathrm{nA}\frac{\delta}{\partial \theta_m}\left(\int_A B \cdot \bar{n} dS\right)$$

Where n is the number of windings composing a coil, A is the area of a winding, and B is the magnetic flux density of the rotor. Hence, defining N_i as the fraction of damaged windings of the i-th phase:

$$R_i = N_i R$$

$$L_i = N_i^2 L$$

$$k_e^{(i)} = N_i k_e$$

where $R_i, L_i, k_e^{(e)}$ are respectively resistance, inductance and normalized counter electromotive force for the I-th phase, while R, L, k_e are the same quantities referred to a non-faulty phase.

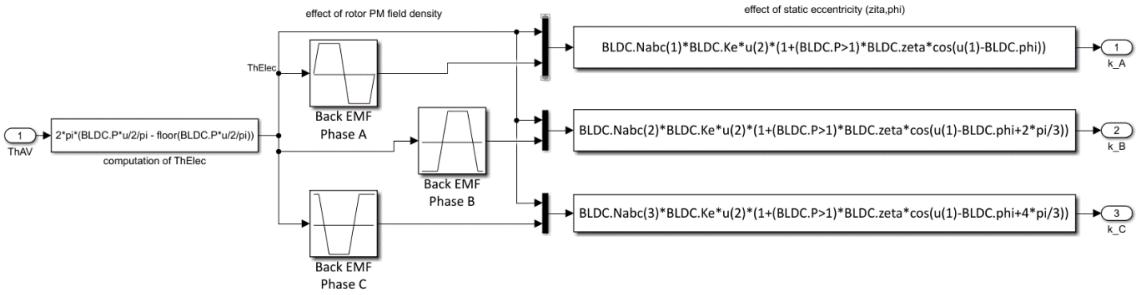

Figure 3.12 – Back-EMF calculation block

2. *SPS - SimScape Circuit conversion Block*: this block performs an ideal conversion between Simulink SPS (Specialized Power System) and SimScape Electrical signal. Current-Voltage Interface block is used. The block act as a current source on the SPS side, and as a voltage source on the Simscape side. To avoid warnings for algebraic loops between the two sides of the converter, a *Memory delay Block* is added on SPS branch, since the voltage measured from the SPS side is used to be fed at the same simulation step to the SMS side to evaluate currents that vice-versa will be passed on the SPS side. A converter block for every phase is used, with a delay of one simulation step.

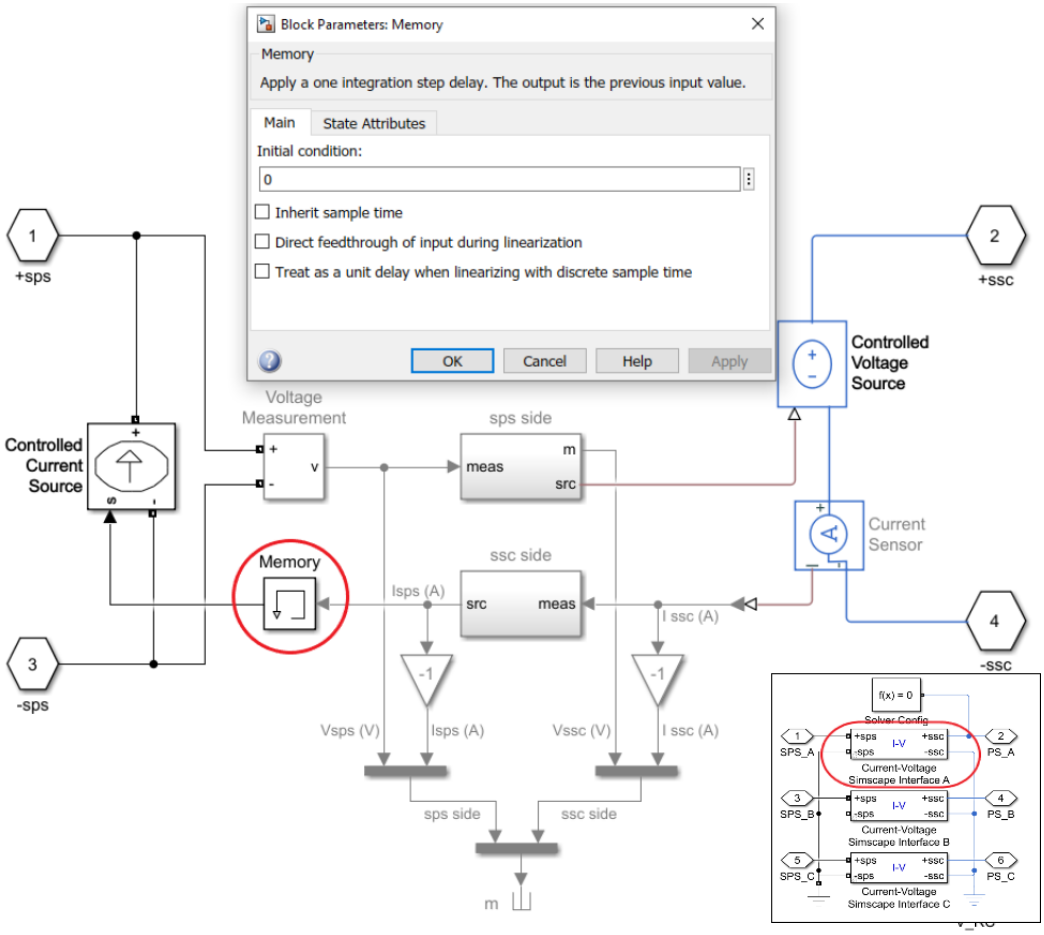

Figure 3.13 – SPS- Simscape Electrical conversion block

3. *Three-phase RL* Block: this block has been remodeled with Simscape Electrical, hence the necessity to have the Current-Voltage interface block, to allow the use of the *Resistor* component with Thermal Port

input. This block models a resistor with optional tolerance, operational limits, fault and thermal noise, but the most important feature is the thermal port Input which allows to have a simple interface between the thermal and the electrical network in order to model how the thermal behavior of the windings influences the performance of the motor. The proposed scheme is a star three-phase connection with RL load on every phase. On each phase is active a voltage generator to represent the Normalized BEMF. Phase current, phase voltages and the voltages at every resistor (V_RA, V_RB, V_RC) are measured; this is both for post-processing and visualization in the model. In future works for prognostic application the phase current will then be converted to an equivalent current to be compared to the current of a single-phase motor from a Monitor model.

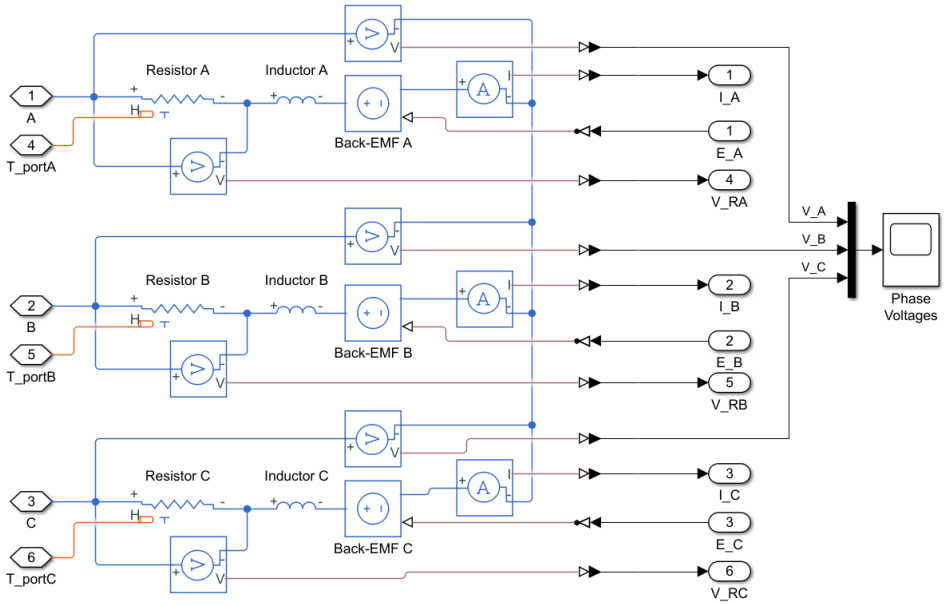

Figure 3.14 – Three phase RL block

4. *Computation of Motor Torque*: this subsystem uses phase currents and normalized counter electromotive forces to evaluate torque delivered by the motor; contribution of the three phases are summed to obtain the resultant torque, which is limited to consider the saturation of magnetic flux in the stator core.

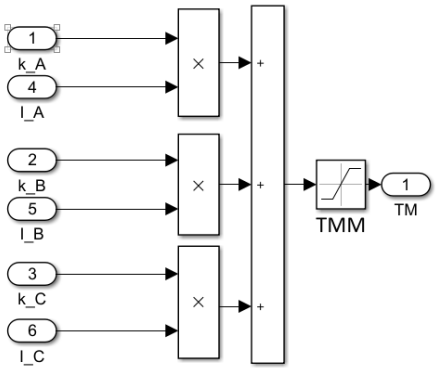

Figure 3.15 – Computation of motor torque

3.1.7 *Motor Transmission Dynamic* Model

This Block models the non-linear transmission dynamic, with fault simulation capabilities. Torque Load and Motor Torque are given as input

signal. Therefore, the resultant is computed after the application of Viscous Torque – equal to zero if the motor is still – and Dry Friction Torque, which is modelled based on Borello Friction model.

This numerical model has little computational effort and is a substitute to most of the dry friction models such as Karnopp and Quinn. It allows to assign a sign to the friction torque depending on speed direction, it allows to distinguish between stick conditions (static) and dynamic friction, enabling the choice between the two friction coefficients and it is capable of evaluating the stop of an initially moving mechanical component; on the other hand it can evaluate the start of an initially stopped component. The mathematical model is the following:

$$\mathrm{F_f} = \begin{cases} F_{act} & x = 0 \wedge |\dot{F}_{att}| \leq F_{sJ} \\ F_{dj} \cdot sg\,n(F_{act}) & \dot{x} = 0 \wedge |F_{att}| > F_{sj} \\ F_{dj} \cdot sgn(\dot{x}) & \dot{x} \neq 0 \end{cases}$$

Where F_f is the calculated friction force, F_{act} is the active force applied to the system, F_{sj} is the friction force in stick condition and F_{dj} is the friction force in dynamic condition. This model has a zero-crossing detection algorithm on the velocity signal, in order to detect when the moving component is stopping its motion. Every time the zero-crossing routine gives a positive output the speed is then set to zero in the following integration step. In this step the resultant torque is then compared to static friction: if the result is positive the component starts again to move, otherwise it will sty still. In conclusion, Borello model avoids the use of non-physical parameters like Karnopp's dead-band or Quinn's hyper-viscous coefficient. On the other hand, Borello introduces a lag of half-time step during velocity reversal, due to the signal reset on zero-crossing [6].

After the evaluation of active torque acting on the shaft, the acceleration is then computed by mean of slow shaft inertial load and motor moment of Inertia (constructor parameter). Note that the transmission is supposed to be infinitely stiff since a term proportional to shaft rigidity is missing.

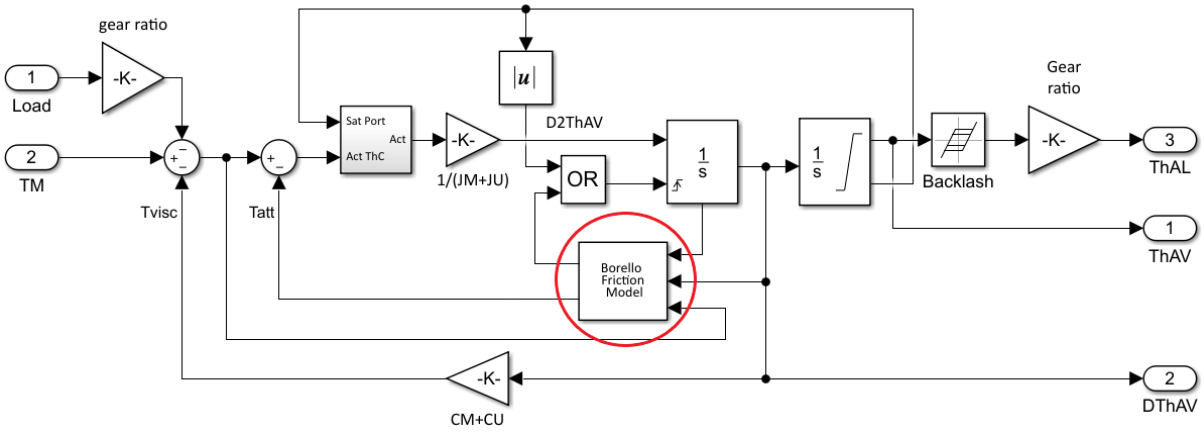

Figure 3.16 – Motor Transmission Dynamic Block

The second fault which is introduced in the *Motor Transmission Dynamic* Block is the backlash due the wear of the mechanical component responsible for motion transmission (i.e. ball bearing or ball screw/nut) between motor and user. The transmission is usually performed through these components that have a small amount of play between the moving parts to allow for components relative motion. This play is managed by manufacturers through specific tolerances and a certain amount of preload. The preload has the downside of increasing the friction an so the wear of all moving components and a certain downgrade of the transmission efficiency due to the decrease of the useful available power. In Figure 3.17 it is shown the backlash that occurs in a section of a ball bearing, where the backlash influences the contact angle ψ.

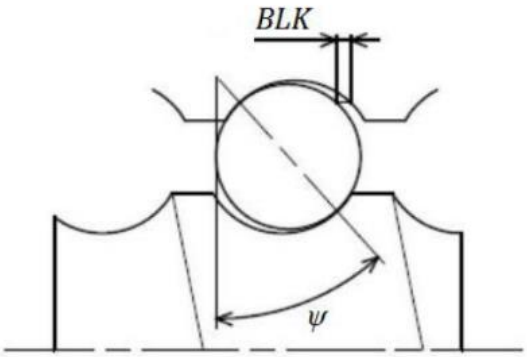

Figure 3.17 – Backlash in a ball bearing

Backlash fault can interfere with the control law, causing a reduction of positioning precision proportional to the backlash module and in some cases dynamic instability through the interaction with an integrative gain, leading to a limit cycle.

4. Thermal Model

In permanent magnet brushless DC motors – as in all electric machines – the power losses that determine the thermal behavior come from sources of different nature and govern performances, response and remaining useful life of the whole system. In many situations the performance and efficiency are even constrained by the thermal dynamics: a machine with an underestimated cooling system may enter a protection state to prevent possible faults or damage even in the nominal operating conditions.

During the design of the electromagnetic machine, even the choice of the material for the permanent magnet must consider or, at least go side by side, with the thermal analysis, to avoid crossing the demagnetization temperature. The best results can be obtained using software for multi-domain physical simulation. Although this software is mostly used in a more advanced phase of the design process, because of the computational cost and time required.

Furthermore, this type of simulation is not suitable for real-time application such as prognostic. For the afore-mentioned reasons we propose a lumped parameter model to be implemented in Simscape Environment. The implementation in Simscape environment went along with a validation of the BLDC motor with manufacturer available information and a Thermal Finite Element Analysis in Autodesk Inventor NASTRAN environment.

The FEA analysis was adopted mostly to gain confidence on the analytical/lumped parameter model and to show the temperature rise of the BLDC motor. Note that both a steady-state and a transient analysis are performed in order to extrapolate thermal inertia characteristics of the motor and having the opportunity to coherently evaluate the results.

4.1 Thermal losses in electric machines

The thermal problem in electric machines is highly complex and its dependency on the fluid-dynamics of the motor as a whole, as well as on the electro-magnetic components (windings-magnets) and on mechanical components (shaft, case geometry, bearings) makes it really difficult to develop a model that can simulate properly and in complete way the thermal behavior of the motor. For these reasons, the optimal solution is to develop models, be them real-time or more "complete" CFD and Electro-Magnetic FEM models, that suits the peculiar application and/or the specific motor performances that needs to be studied.

The goal of this thesis is to build and integrate in an already high detailed model, the thermal behavior of BLDC Motor. This preliminary model must be suitable for Prognostic algorithms (be it Genetic algorithms or Artificial Neural Networks) to perform a fault detection routine. These are the main losses linked to the thermal behavior of the BLDC motor:

- *Excitation current losses*: they are strictly related to the load conditions, since currents vary widely to keep the voltage at the stator winding to a constant value;

- *Mechanical losses (friction and ventilation)*: as already mentioned before, the mechanical transmission of motion has a certain value of efficiency due to losses in power in component like bearing and nut/screw coupling caused by friction. A BLDC motor is affected in the same way by this problem as the shaft that holds the rotor magnet is usually supported by two or more bearings. The number and the type of bearings depends on the size of the motor and its capability to sustain axial and/or radial loads. Typically, the motor bearings have a higher range of velocities respect the ones supporting the ball screw and their lubrication status needs to be kept under control to avoid inefficiencies. These types of losses are quite moderate compared to *eddy current* and

Joule effect losses and are relatively difficult to model, given their strict dependency upon bearing geometry, wear and lubrication state.

- *Eddy currents (Foucault effect)*: according to Faraday's law of Induction, when a coil of conductive material is immersed in time-varying magnetic a field, a current is induced that circulates inside the conductor, if there is a closed loop. In analogy with this principle, when a conductive mass is subjected to the same magnetic field, we can observe a similar current, but with circulation loop that starts and finish inside the material. These are referred to as eddy currents. Effect of these currents are the production of due to *Joule effect*, the generation of a reaction magnetic field and they produce forces due to the interaction of the inducing and the induced field.

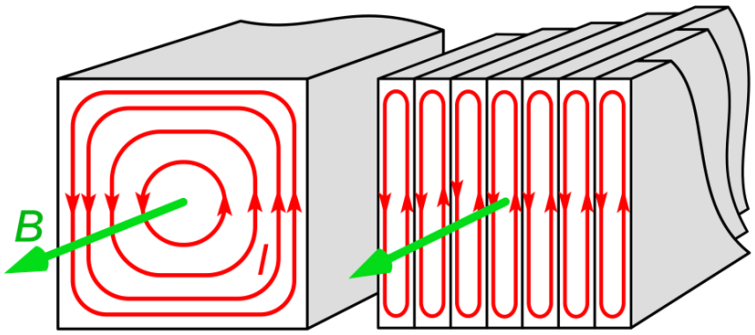

Figure 4.1 – Eddy current in non-laminated and laminated material

In electrical machines almost all the components are subjected to time-varying fields, stator and rotor included. In the rotor of BLDC motor this effect appears in the rare elements magnet and if it's not considered in the design phase there is the risk of demagnetization of the rotor. In the analysis from [12] it is shown this behaviour: *"[...] rotor eddy current loss is relatively low if compared with the motor power. Hence reduction of the rotor loss is not so meaningful for the motor power efficiency. However, the rotor eddy current loss may cause rather high*

temperature in the rotor, such that the magnets may be demagnetized. Therefor it is crucial to reduce the rotor loss."

A reference equation for evaluating the eddy current losses in an ideal component (a wire or a sheet of metal) is:

$$P_E = \frac{\pi^2 B_p^2 d^2 f^2}{6 k \rho D}$$

Where P_E is the power loss per unit mass [W/kg], B_P is the peak magnetic field [T], d is the thickness of the sheet or diameter of the wire [m], f is the frequency [Hz], k is a constant equal to 1 for a thin sheet and 2 for a thin wire, ρ is the resistivity of the material [Ω m] and D is the density of the material [kg/m³]. This equation is only valid under the hypothesis of uniform material, uniform magnetic field, no skin effect and can't be used to model this phenomenon in a high dynamic time varying system as a BLDC motor.

- *Joule effect*: this is the effect that is going to be modeled to reproduce the winding heating during motor operations. Assuming that on every phase of the three-phase motor we a have a loss of energy due to the resistive load, then we can assume the total loss on every i-th branch of the motor to be equal to:

$$P_{JE}^{(i)} = V^{(i)} \cdot i^{(i)}$$

using instantaneous values for all electrical quantities and substituting the characteristic equation of the ideal resistor $V(t) = R(t)i(t)$, we obtain:

$$P_{JE}^{(i)}(t) = R^{(i)}(\mathrm{T}) \cdot i^{(i)}(t)^2$$

Where $P_{JE}^{(i)}(t)$ is the instantaneous power loss at time t of the simulation (or from the Simscape model point of view, the Heat Flow in the node adjacent the winding coil) on the i-th phase [J/s], $R^{(i)}(T)$ is the

resistance value depending on temperature [Ω], $i^{(i)}(t)$ is the instantaneous current value at time t on the i-th phase of the motor [A].

4.1.1 Electric-thermal coupling: Resistance

The resistivity of a material, an electrical winding in particular, depends on length, section, and composition but changes with temperature depending on the following equation:

$$\rho(\mathrm{T}) = \rho_0[1 + \alpha\,(T(t) - T_0)\,]$$

Where $\rho(T)$ is the resistivity [Ω m], $\rho_0(t)$ is the reference resistivity at standard temperature (298,15 K), α is the linear temperature coefficient (for copper $\alpha = 0{,}00404$ 1/K at 293,15 K), $T(t)$ is the resistor temperature [K] at time t of the simulation and T_0 is initial winding temperature [K] at standard temperature. The resistance depends in the same way from temperature:

$$R(T) = R_0\,[1 + \alpha\,(T(t) - T_0)\,]$$

$R(T)$ and R_0 are value [Ω] and initial resistance at standard temperature [Ω].

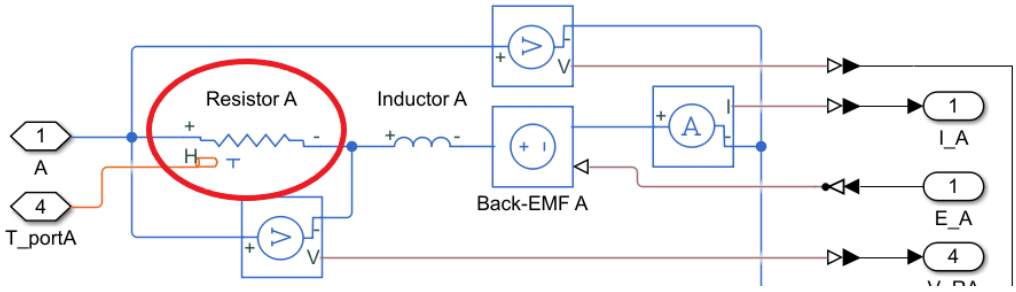

Figure 4.2 – Single RL branch of the three phases BLDC motor model

As mentioned in the previous paragraph, the thermal state of the motor influences also the RL branches of the electrical network. This behaviour is taken into account using a temperature-depending resistor block with

thermal port. This block is the node to integrate the two physical networks, since it uses the above-mentioned relationship to compute the resistance value and refreshes at every simulation step. The following equation describes the thermal behaviour of the block:

$$P(t) = \mathrm{K_d t_c} \frac{dT(t)}{dt} - i^2(t)\, R(T)$$

Where $P(t)$ is the heat flow through the port H [J/s], m is the mass, c_p is the specific heat, dT/dt is the rate of change of the temperature, i is the current value [A]. The $K_d t_c$ product is equal to the thermal mass of the winding so it is passed through parameters window as the product of specific copper heat C_p and windings mass m_w, which is approximated through the Finite Element Method Thermal Analysis.

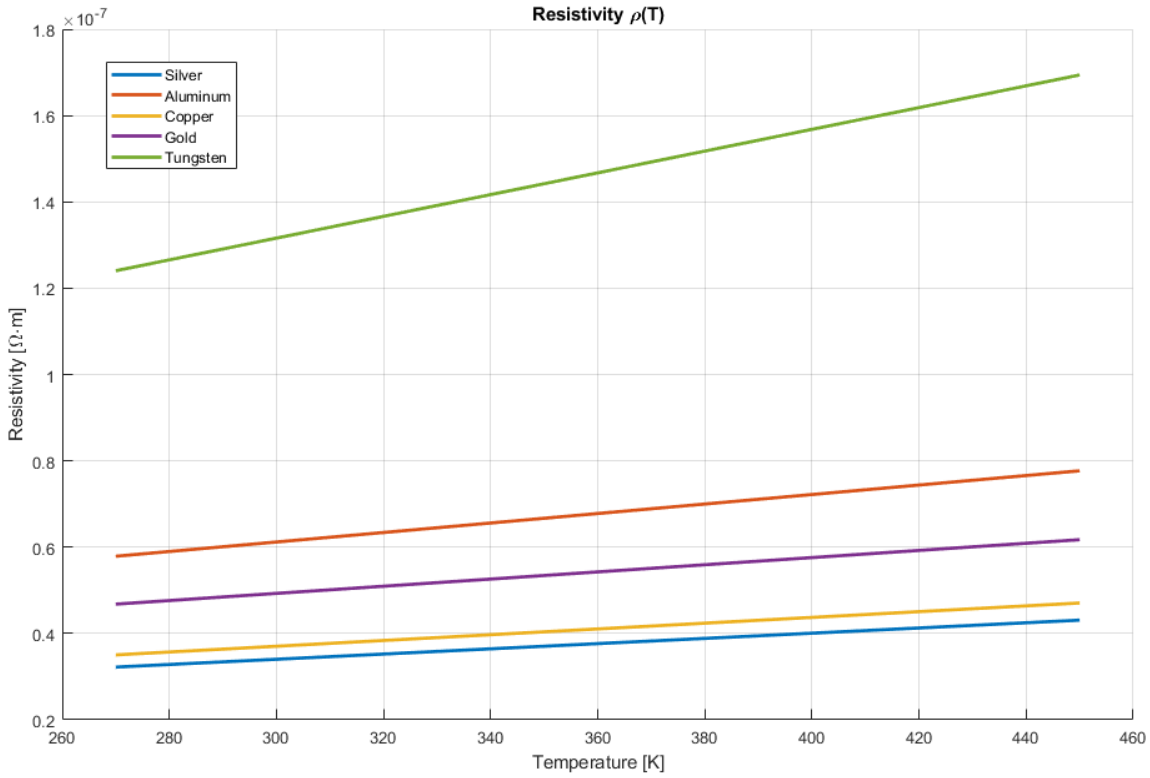

Figure 4.3 – Resistivity with temperature

To quickly show how $R(T)$ variation affect the dynamic of the motor both mechanically and electrically, let's consider a simple brushless DC motor

where the KVL is applied to derive the "total" voltage equation and coupled with torque relation. The derived response applies to all servomotor including brushless dc, ac induction and variable reluctance motors with both linear and cylindrical geometry.

Briefly considering the voltage equilibrium equation applied to a phase of the motor as V_{DC}[13]:

$$V_{DC}(t) = L\frac{di(t)}{dt} + i(t)\cdot R(T) + K_E(T)\cdot\omega(t)$$

Where $V(t)$ is the applied voltage command [V], t is time [s], L is motor's inductive load [H], $i(t)$ is motor current [A], T is the winding operating temperature [K], $R(T)$ is motor's resistive load at given temperature T, $K_E(T)$ is Back EMF constant [V/rad s] at given temperature T (this dependency will be discussed in the Section 4.1.2) and $\omega(T)$ is motor speed [rad/s]. Followed with the torque equilibrium equation:

$$K_T(T)\cdot i(t) = J_M\frac{d\omega(t)}{dt} + C\cdot\omega(t) + F_f$$

$K_T(t)$ is the torque coefficient (also considered to be temperature varying as K_E) [Nm/A], J_M is motor moment of Inertia [kg m^2], C_M is the viscous coefficient for viscous friction and F_f is dry friction (see Chapter 3 for details in Dynamic Mechanical model Section) [Nm]. Note that the viscous friction coefficient and dry friction force might incorporate both phenomena for motor and load; in that case the moment of inertia also has to take into account the load's inertia. In the torque equation, after assuming viscous friction load to be null, we isolate the current and substitute the resulting in the voltage equilibrium equation obtaining, after normalizing with Back EMF coefficient:

$$\frac{V(t)}{K_E(T)} = \frac{L\,J_M}{K_E(T)\,K_T(T)}\frac{d^2\omega(t)}{dt^2} + \frac{R(T)\,J_M}{K_E(T)\,K_T(T)}\frac{d\omega}{dt} + \omega(t) + \frac{R(T)\,F_f}{K_E(T)\,K_T(T)} \qquad (1)$$

Mechanical τ_m [s] and Electrical τ_e [s] time constant are then defined as:

$$\tau_e = \frac{L}{R(T)}$$

$$\tau_m = \frac{R(T) \cdot J_M}{K_E(T)\, K_T(T)}$$

With this notation the equation (1) can be rewritten as follows:

$$\frac{V(t)}{K_E(T)} = \tau_m \tau_e \frac{d^2\omega(t)}{dt^2} + \tau_m \frac{d\omega(t)}{dt} + \omega(t) + \tau_m \frac{F_f}{J_M}$$

The four components the determine the motor dynamic response are (except $\omega(t)$) all temperature dependant since the corresponding τ_m and τ_e are as well. With a rise of 105 degrees in a phase temperature raises its Resistance value by a factor of 1,412. The mechanical time constant increases as well by the same factor while the electrical time constant decrease by that factor and this changes how the motor responds to a command. In datasheet, the motor manufacturers specify a time constant values for a given reference temperature (the motor used in this thesis specify a 295 K value). Motor are also related to with a thermal insulation classes (Figure 4.4) [14-15], which defines the Estimated Life of an insulation system based on nominal temperature operations. Based on this information we assumed that a motor can withstand a winding peak temperature of even 130°C (Class B), 155 °C (Class F) to 180°C (class H), thus stressing even more the importance of considering a variation of time constant during operations.

Motor Insulation Temperature Ratings (NEMA)		Temperature rises			
Class	Temperature [°C]	Ambient temperature[°C]	Hotspots [°C]	Rise at SF 1.0 [°C]	Rise at SF 1.15 [°C]
A	105	40	5	60	70
B	130	40	10	80	90
F	155	40	10	105	115
H	180	40	15	120	-

Table 4.1 – Thermal insulation classes

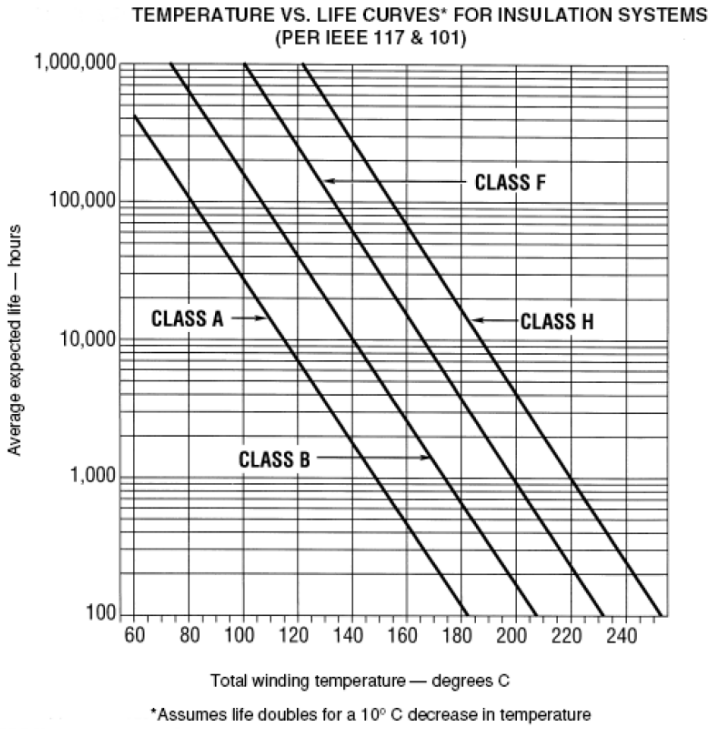

Figure 4.4 – Temperature vs. life cycle for insulation systems

4.1.2 Electric-thermal coupling: K_E and K_T.

One of the most common material for rotor magnets in Brushless DC motor is NdFeB because it offers a good balance between cost and performances (based on inexpensive Iron and Neodymium, one of the most abundant rare

earth element). Magnets made by this material have a coercivity (the ability of a ferromagnetic material to withstand an external magnetic field) of about 800-950 kA/m [16] and a residual flux density (magnetization in a ferromagnetic material after an external magnetic field is removed) of about 1 – 1.3 T (10 000 – 13 000 G) [17]. The disadvantages of this material it's its sensitivity of magnetic properties to temperature, which can worsen motor performances.

The residual magnetic flux B_r and induced field intensity H_c decrease inversely with magnet temperature following [18]:

$$B_r = B_{r0} \cdot \left[1 + \frac{\alpha_B}{100} \cdot (T_{mag} - T_0)\right]$$

$$H_c = H_{c0} \cdot \left[1 + \frac{\alpha_H}{100} \cdot (T_{mag} - T_0)\right]$$

where T_{mag} is the magnet temperature (not equal to winding temperature during transient response, but catching up with a lag), T_0 is staring temperature of the magnet, B_{r0} and H_{c0} are the residual flux density and coercive field intensity at temperature T_0, $\alpha_B < 0$ and $\alpha_H < 0$ are temperature coefficients for B_r and H_c expressed in [% / K]. In these equations it shown the dependency of demagnetization properties on magnet temperature: the magnetic coupling between stator winding generated magnetic flux and rotor NdFeB magnet is then used in the computation of K_E and K_T.

In the thermal model this effect won't be introduced since T_w (windings temperature) is the temperature influenced by Joule effect and the two values are very different in non-stationary conditions and due to the complexity of the motor internal geometry and dependency of B_r upon air gaps between magnets and stator coil and upon magnet geometry, so, again, a dimensional parameter that is not given by the manufacturer.

4.2 Lumped Parameter Modeling Scheme

4.2.1 Generic Formulation

A lumped parameter element is a discrete object that can exchange energy with other object of a lumped parameter network in which it is placed and whose internal physics can be combined into "terminal" relationship (e.g. an ideal resistor). Another assumption for this object is that the its size must be smaller than wavelength of the appropriate signal which means that the signal does not take time to propagate. Every element has one or more ports, each port is associated with two variables: a "through" variable and an "across" variable: an ideal resistor has current and voltage, an ideal spring has displacement and force, an ideal thermal resistor has heat flow and temperature. Note that in all the three elements the power into the port is defined by the product of these the two variables.

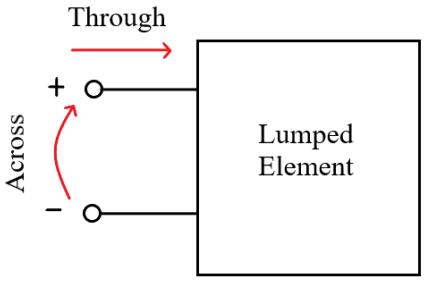

Figure 4.5 – A lumped parameter element

Among all equivalent lumped elements, the most interesting are the electrical ones since we can represent any physical domain network as an equivalent electrical network and use the Kirchoff's Current Law and Kirchoff's Voltage Law to solve them. For this to be feasible we need that every physical domain network must have elements connected in a way that the conservation/congruence laws are intrinsically observed (i.e. Newton's Law for mechanical domain, Conservation of Energy for thermal domain, Mass conservation for fluid-dynamic domain, etc...). If these assumptions are

respected every domain have one representation to be solved. Introducing generalized variables for lumped parameter modeling of passive components:

- *Flow:* $f(t) = \frac{dq}{dt}$
- Displacement: $q = q_0 + \int_0^t f\, dt$
- *Effort*: $e(t) = \frac{dp}{dt}$
- *Momentum*: $p(t) = p0 + \int_0^t e\, dt$
- *Net power into device is effort times flow:* $P_{net} = e \cdot f$

Combining the previous relationships, we can have three general **passive** elements:

- *Resistor* - relates *e* and *f* directly (effort is an algebraic function of flow):

$$e(t) = R \cdot f(t)$$

- *Capacitance* - relates *e* and *q:* $f(t) = C \cdot \frac{de(t)}{dt} = C \cdot \frac{d^2p(t)}{dt^2}$
- *Inductance* – relates *f* and *p:* $e(t) = L \cdot \frac{df(t)}{dt}$

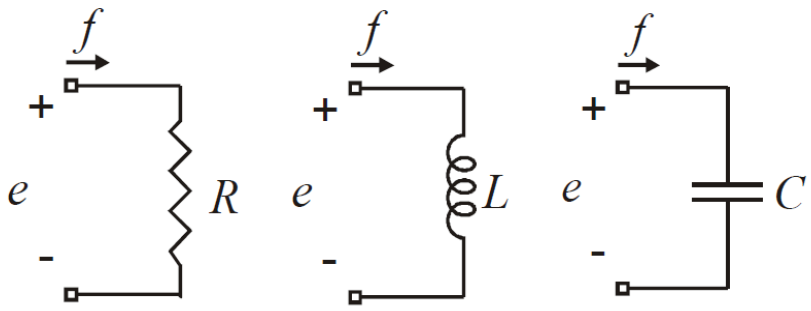

Figure 4.6 – Passive elements of a lumped parameter model

To better understand the generalization, we can make an example of the equivalence between electrical and mechanical domain, before proceeding to show the thermal lumped parameter network for the BLDC motor. Let's consider a resistor from electrical domain: its equivalent is a mechanical viscous damper. The resistor responds to Ohm law $V(t) = R \cdot i(t)$ (V voltage, R resistance, i current) and the damper responds to $F(t) = b \cdot v(t)$ (F force, b

damping coefficient, *v* velocity). Referring to the general case, *V(t)* in the resistor and *F(t)* in damper are the *effort* variables and *i(t)* and *v(t)* are the *flow* variables. *R* and *b* are correspondent constants.

In the same way, we can consider a capacitor in electrical domain and a spring in the mechanical: the first relates the change of voltage at terminal to the current flowing to it with $i(t) = C \cdot \frac{dV(t)}{dt}$ and the latter can be either considered with the well know relation $F(t) = k \cdot x(t)$ or for our purpose it can be derived and rearranged as:

$$\frac{dx(t)}{dt} = \dot{x}(t) = v(t) = \frac{1}{k} \cdot \frac{dF(t)}{dt}$$

Where, again *v(t)* is the spring velocity, *F(t)* is the spring compression force and *1/k* represents the equivalent capacitance. Note that both components are a "storage" of potential energy. If a voltage is applied to the electrical capacitor terminal, the plates accumulate charge and when tension is changed (e.g. a switch is closed) that same energy gets released in form of current. In the same way a spring stores potential elastic energy when a force is applied to its ends and releases it as soon as the force keeping it compressed (or lengthened) is removed; the way of releasing energy in this case is in form of velocity and only when the spring is still it can be considered properly "discharged".

To complete the equivalence between the two domains let's consider an ideal inductor from electrical domain which defining relation is:

$$V(t) = L \cdot \frac{di(t)}{dt} = L \frac{d^2Q(t)}{dt^2}$$

with L as the ideal impedance value. In mechanical domain it is paired with an inertial mass which constituting equation is $\mathrm{F(t)} = \mathrm{m} \frac{\mathrm{d}v(\mathrm{t})}{\mathrm{dt}}$. Considerations that has already been made for the other two equivalent passive components are valid in this case either.

A lumped circuit, along with electrical equivalence, needs also some **active** components that function as ideal power sources. In the general picture there are two types: the *Ideal Effort* source and the *Ideal Flow* source. The first establishes a time-dependent *effort* independent of flow (e.g. ideal electrical voltage generator, ideal pressure source) and the latter establishes a time-dependant flow independent of *effort* (e.g. electrical current source and pump).

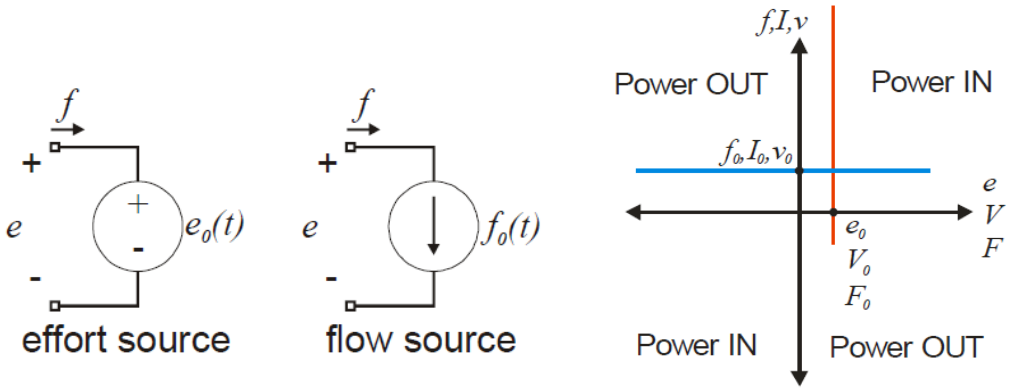

Figure 4.7 – Active element of a lumped parameter model

Once the components are defined, they need to be arranged in a lumped according to the conservation/congruence laws proper of every domain. The elements that share *flow* (e.g. current) and displacement (e.g. charge) are placed in series in an electric circuit. The elements that share a common *effort*. (e.g. Voltage) are placed in parallel in an electric circuit. The same rules are applied to other domains according to the generalization of variables. In this way, as shown in Figure 4.8, a Spring-Mass-Damper system can have an equivalent circuit.

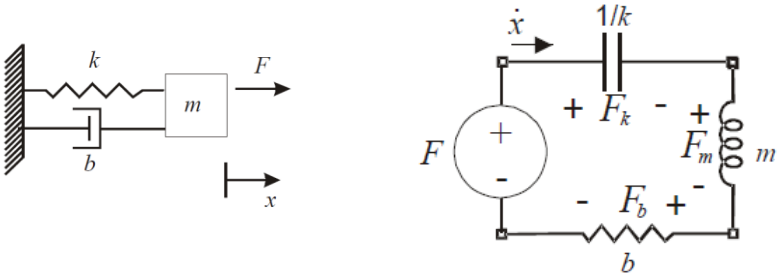

Figure 4.8 – MSD system and the equivalent lumped parameter model

Applying force balance to a SMD system in the left of Figure 4.8 as follow:

$$\sum_{i} F_i(t) = m \cdot a(t) \quad \Rightarrow \quad F(t) - kx(t) - b\dot{x}(t) = m\ddot{x}(t)$$

Grants the same results as applying Kirchoff's Voltage Law to the circuit on the right in the same figure:

$$F(t) - F_k(t) - F_m(t) - F_b(t) = 0$$

$$F(t) = kx(t) \;\; ; \;\; F_b = b\dot{x}(t) \;\; ; \;\; F_m = m\ddot{x}(t)$$

$$F(t) = kx(t) + b\dot{x}(t) + m\ddot{x}(t)$$

General	Electrical	Mechanical	Fluidic	Thermal
Effort (e)	Voltage, V	Force, F	Pressure, P	Temp. Difference,
Flow (f)	Current, I	Velocity, v	Vol. flow rate, Q	Heat flow, P
Displacement (q)	Charge, Q	Displacement , x	Volume, V	Heat , Q
Momentum (p)	-	Momentum, p	Pressure momentum, Γ	-
Resistance	Resistor, R	Damper, b	Fluidic resistance, R	Thermal resistance
Capacitance	Capacito, C	Spring, k	Fluid capacitance, C	Heat Capacity mcp
Inductance	Inductor, L	Mass, m	Inertance, M	-
Node Law	KCL	Continuity of space	Mass conservation	Heat energy conservation
Mesh Law	KVL	Newton's 2nd Law	Pressure is relative	Temp. Is relative

Table 4.2 – General lumped parameter formulation

4.2.2 Thermal domain formulation

Applying all the previous concepts to thermal domain we obtain: temperature *T(t)* becomes the across variable (*effort* type of variable), heat-flow *P*

becomes the through variable (*flow* type of variable) and the conserved quantity is the heat energy. Passive elements are:

- *Thermal Resistor*: this component represents an abstract quantity that relates the thermal conductivity, the heat transfer coefficient, and the radiation coefficient. It models heat transfer in generalized terms independent of whether it is by conduction, in which case the value of Resistance will be $R = \frac{D}{k \cdot A}$, convection with $R = \frac{1}{h \cdot A}$, radiation $R = \frac{1}{r \cdot A \left(T_A^2 + T_B^2\right)(T_A + T_B)}$ or a combination (D is the material thickness, that is, distance between layers, A is area normal to the heat flow direction, k is thermal conductivity of the material, h is convection heat transfer coefficient, r is radiation coefficient, T_A and T_B at ports A and B respectively).

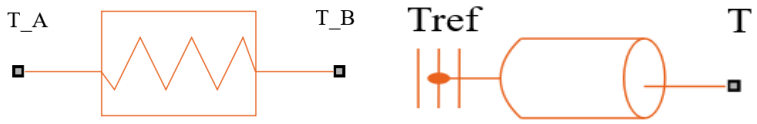

Figure 4.9 – Thermal passive components

- *Thermal Mass (Heat capacity)*: this component represents a thermal mass, which reflects the ability of a material or a combination of materials to store internal energy. The property is characterized by mass of the material and its specific heat. The thermal mass is described with the equation $Q = c \cdot m \frac{dT}{dt}$ where Q is the heat flow, c is the specific heat of mass material, m is the mass and dT/dt the variation of temperature with time. Note that in the Figure 4.9 the block is shown

with two port: T on the node relative to the material temperature and T_{ref} relative to the reference temperature for the thermal network.

The other active components are:

- *Heat flow rate source*: the component represents an ideal source of thermal energy that is powerful enough to maintain specified heat flow at its outlet regardless of the temperature difference across the source.
- *Temperature source*: this component represents an ideal source of thermal energy that is powerful enough to maintain specified temperature at its outlet regardless of the heat flow consumed by the system. The source generates constant absolute temperature, defined by the "temperature" parameter value. As in the case of the thermal mass, one of the nodes of this block is on a T_{ref} node.

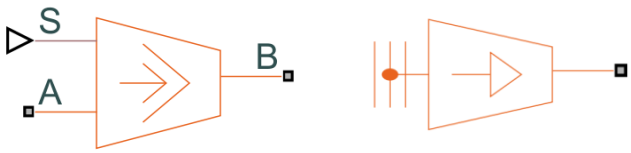

Figure 4.10 – Thermal active components

4.3 *Thermal Model* Block

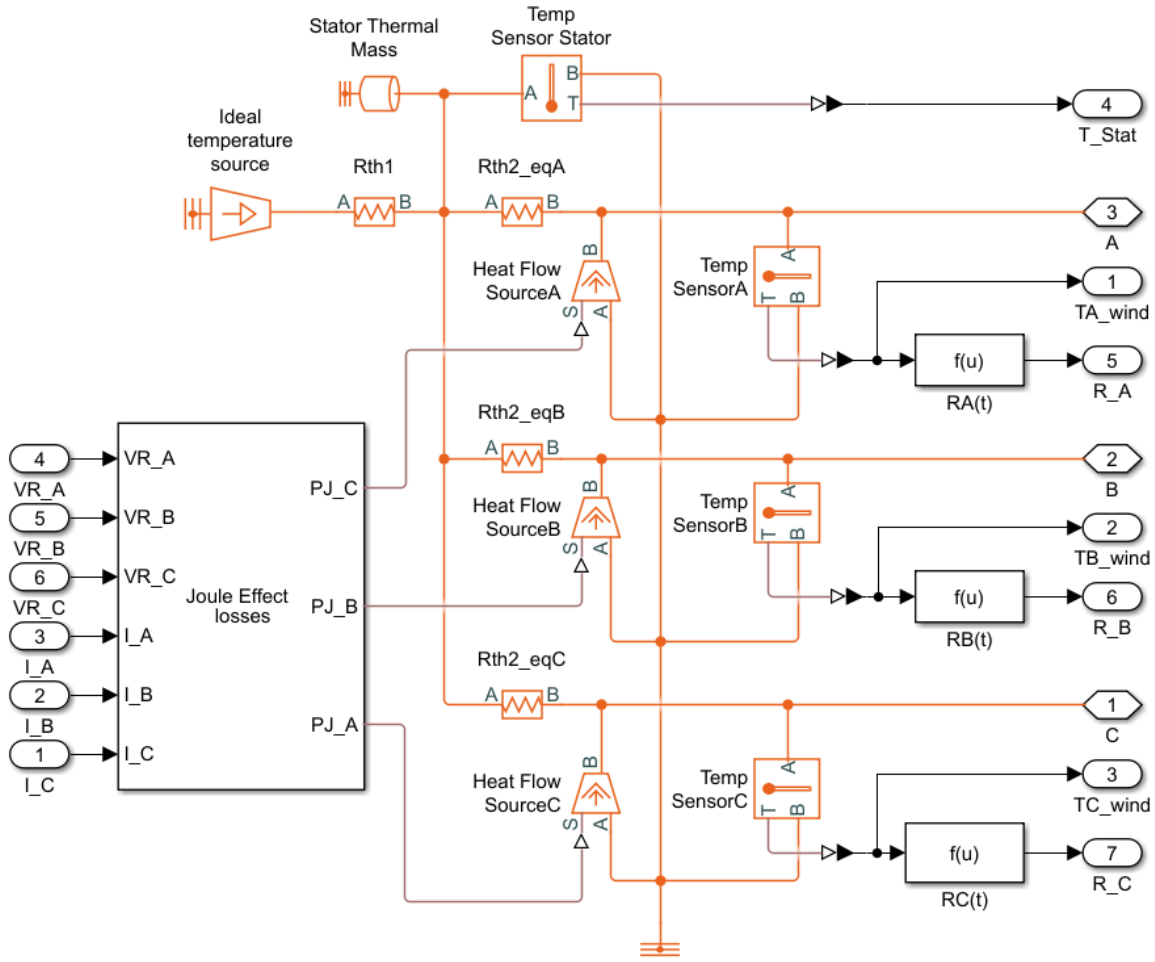

Figure 4.11 – Thermal model Block

This block models the thermal behavior of the three-phase BLDC motor. As in the electrical branch shown in Chapter 3, this model also has three branches thermally coupled with the stator case. In Figure 4.11 four thermal resistances are shown: `Rth1` and `Rth2_eqA`, `Rth2_eqB`, `Rth2_eqC`. ***Rth1*** is relative to the convective exchange between the stator aluminum case and the external air (natural convection is assumed). `Rth2_eqA`, `Rth2_eqB`, and `Rth2_eqC`, represents the heat exchange between stator windings and stator case; note that they all have the same value since the motor phases are supposed to be assembled with the same geometry and have all the same air gap to the stator. In addition to resistances the model has two thermal

capacities, to model the thermal energy storage of two components of the motor: the stator case and the windings. The stator mass has been estimated through a thermal Finite Element Analysis that is shown in section 4.5. The mass of the windings has been approximated after a second FEA analysis since only the manufacturer has the exact data and the geometry of the motor. Winding mass doesn't appear in the thermal block since it is inserted as a parameter directly into the electrical resistor block (see Chapter 3).

A Controlled Heat flow source is inserted on every one of the three thermal branches to feed the system with calculated power loss due to Joule Effect. The power loss is derived at each simulation step from the electrical network and it represents the instantaneous value for every phase: in Chapter 5 will be shown how the three-phase windings will heat depending on the controlled current flowing through them.

The convective exchange between the stator case and the external air is managed through an Ideal temperature source, which functioning has already been explained; with this artifact it is basically assumed that external air temperature never changes disregard of amount of heat that is being exchanged; this is a strong assumption that is only valid when we have a motor mounted on a test bench since in an on-board integrated EMA there is usually smaller air volumes and the temperature can't be considered as a constant, but as a variable (less air means also that considerations about natural convection needs to be suited for the peculiar assembly condition). Nonetheless, in this network we are instead considering an EMA mounted through a metal flange to a support of some kind; the manufacturer explained in the datasheet that if such a mounting condition has to be considered a 25% rise in $Rth1$ must be taken into account since the flange gives an additional way to the heat.

The motor can be represented by a more sophisticated thermal model that considers every component as a thermal resistor itself, modeling even the contact between different component as additional thermal resistances. In

these models, heat has many more flow paths. That is why in order to do the most complete analysis in order to develop a product and detect the boundaries for normal operations, motor designers always produce the most detailed model, including electrical, mechanical, thermal and chemical components. A simpler thermal model is generally of use if there's the need to provide guidelines for thermal protection by evaluating thermal risk with reference to motor data sheet and thermal damage curves. A simple motor model might be also useful in all these applications where the purpose of the analysis is to develop prognostic algorithms that does not requires a computational heavy and detailed motor model to be simulated.

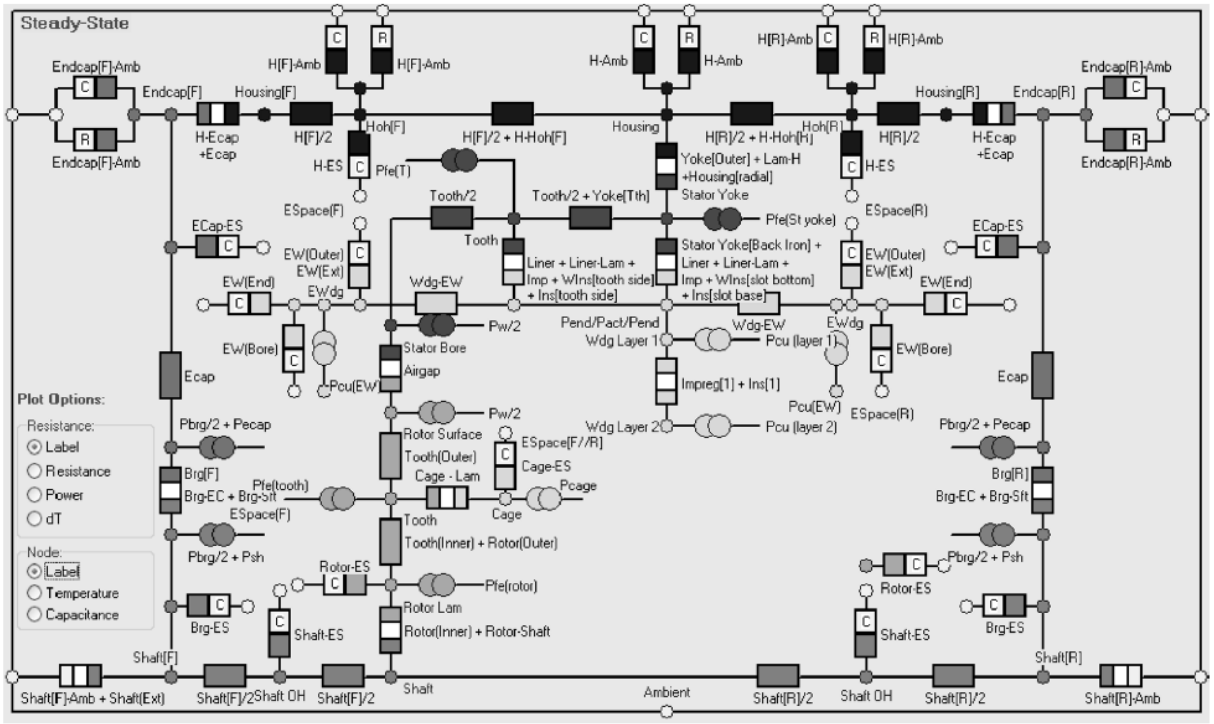

Figure 4.12 – A high detailed motor thermal model (lumped formulation)

4.4 Finite Element Method estimate of Thermal masses

To estimate the aluminum stator case mass (and roughly estimate winding mass) an analysis with a Finite Element Analysis software is performed. Autodesk's NASTRAN Inventor NASTRAN is used. The software is a CAD/CAE tool with an integrated a shell to perform all sorts of common Finite Element Method analysis: from static linear or non-linear to modal analysis of a structure, buckling analysis, thermal steady-state linear and non-linear analysis and thermal transient non-linear analysis.

The process of estimating the thermal masses of the motor starts form a 3D model of the motor that gives the overall dimensions of the motor stator case. This model is not a hollow body so (Figure 4.13), through iterative thermal non-linear transient simulations the geometry is derived matching the thermal time constant to the one given by the manufacturer, which is for the stator case τ_{w2} = 1222 s. The stator mass is then derived from this constant. The FEA simulation steps are listed as follows:

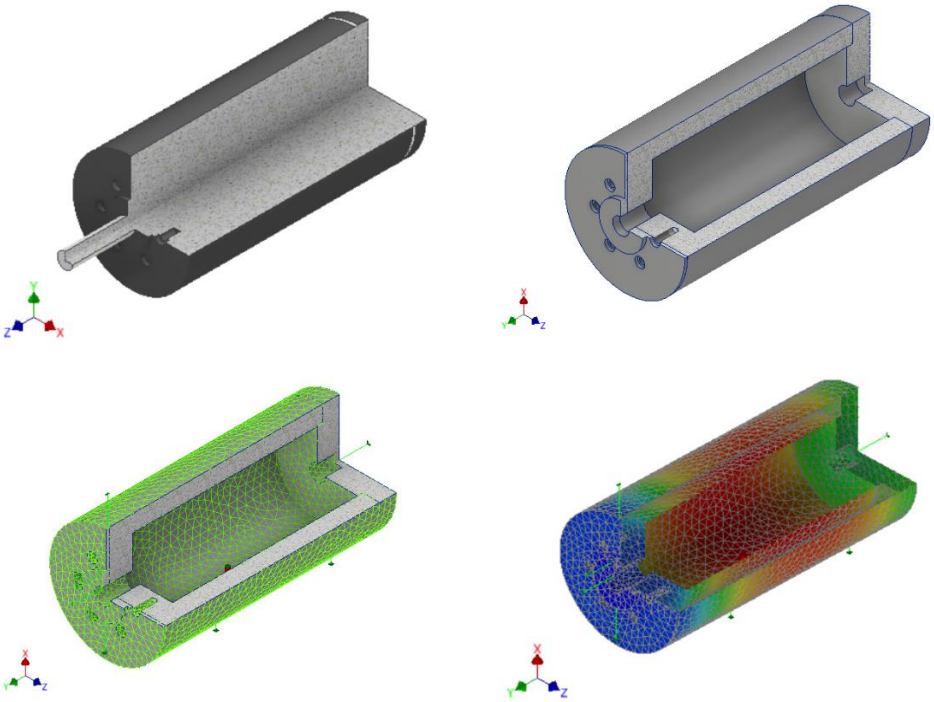

Figure 4.13 – The four steps of the Thermal Finite Element Analysis

1) *Material and Mesh:* as indicated in the manufacturer's datasheets an Aluminium 6061 is chosen for the stator, with thermal conductivity equal to $1{,}67 \cdot 10^{-2}$ W/ (m K) and specific heat 897 J/(kg K). The mesh elements are liner solid element with medium dimension of 5 mm. The dimension of the element is quite rough due the fact that this will be only a transient analysis, keeping trace of the Maximum temperature vs Time. The so generated mesh has a total of 2596 nodes for 9658 elements.

2) *Thermal loads:* the stator is assumed to be directly in contact with the stator windings. This is a simplification that sets a common thermal node, dynamically speaking, at the interface between the two components; in a real model we should consider a thermal resistance that creates a step discontinuity at the interface. We are assuming a heat flow that comes directly after the temperature "step". The input flow heat is set to 3400 W/m^2. The value of the heat flow has been set keeping in mind that the maximum winding and stator temperature is 420K (125 °C, see Table 2.2). The motor is also exchanging heat with environment via convection.

   To properly set the convective load the following assumptions are made: the motor is supposed to not have an external cooling system, so the convection is supposed to be characterized only by a free type of convection (for air h, convective heat transfer coefficient, is typically about $5 - 15\, W/(m^2 \cdot K)$). Thermal resistance R_{th2} given by the manufacturer was 5,2 K/W; from this value the convective heat coefficient for the motor is calculated:

$$h_S = \frac{1}{\mathrm{R_{th2}\,A}} = \frac{1}{0{,}0154\ \mathrm{m^2} \cdot 5{,}2\ \frac{\mathrm{K}}{\mathrm{W}}} = 12{,}48\ \frac{\mathrm{W}}{\mathrm{m^2 K}}$$

   Which is the value that will be used in the convective heat load coefficient in the simulation and in the FEA.

3) *Boundary conditions*: the stator is set to an initial temperature of $T\_0 = 295\,K$, the same used in the Simulink model and used by the manufacturer to rate the motor.

The time constant is $\tau_S = 1120s$, which differs form the datasheet value with about the 8,35% of error. This amount of error is acceptable for the simulation due to the many assumption and an intrinsic inaccuracy of the geometry of the motor stator case. The mass of the stator is derived as:

$$m = \frac{h_S \cdot A_S}{\tau_S \cdot c_p} = 0{,}223\ \text{kg}$$

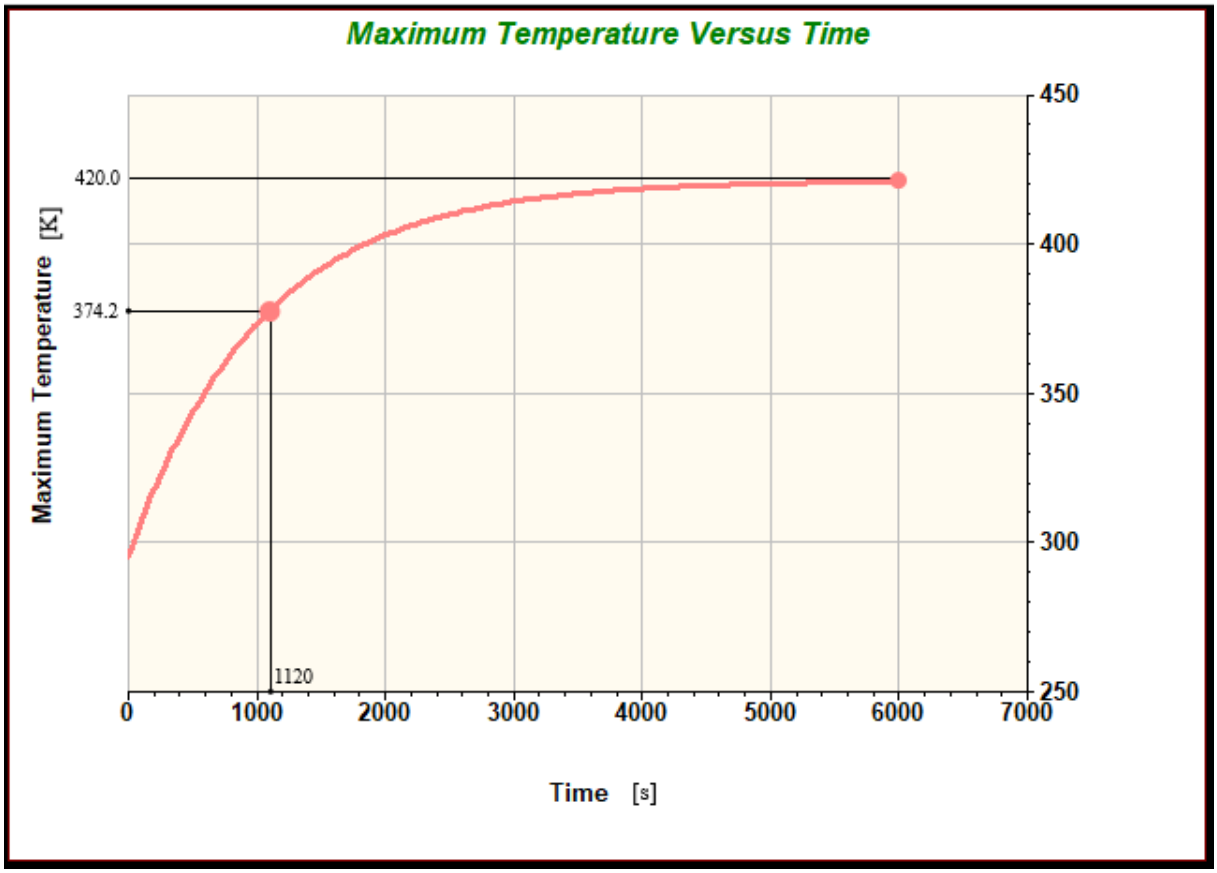

Figure 4.14 – FEA – Transient linear response of the motor

5. Simulation Results

The response of the EMA model is studied under several combinations of loads, command inputs and in nominal no-load and nominal with loads conditions. The aim is to evaluate if the available signals (current and temperature) can be used for prognostic purpose. The three commands analysed for the response are:

- *Step* command at 0,5 s with amplitude of 60° (pi/3 rad): both nominal and faulty state with no-load and secondary-like type surface load;
- *Chirp* command with amplitude of 0,005 *rad* and frequency raging from 0 to 15 Hz:

The step command is used to saturate the controller, so that the dynamics doesn't influence the response of the system. The reference current signal is saturated with its maximum datasheet value almost during all the transient phase and no feedback signal is modifying the control current reference signal.

5.1 Nominal: No fault - No load conditions

In nominal conditions the system is supposed to operate with no faults. These are the reference conditions for evaluate an eventual wear or damage in the system. All the faulty conditions are derived by changing parameters in the model from the non-faulty state.

5.1.1 Step command

In Figure 5.1 it shown the response to a step command of 1 rad, in terms of position of the slow shaft (AL), speed a torque on the Fast shaft (AV). It can be noticed that the controller is sent in saturation, in this way the response is

similar to the one that can be obtained from a ramp command, with the surface catching up to the commanded position at the maximum shaft speed (after reaching it in a brief transitory phase). Note that in the torque graph the Motor Torque has a high frequency ripple due to the PWM control; the same ripple can be observed in the current graph (Figure 5.2), which is then filtered with a using a filter with cut-off frequency of 2 kHz.

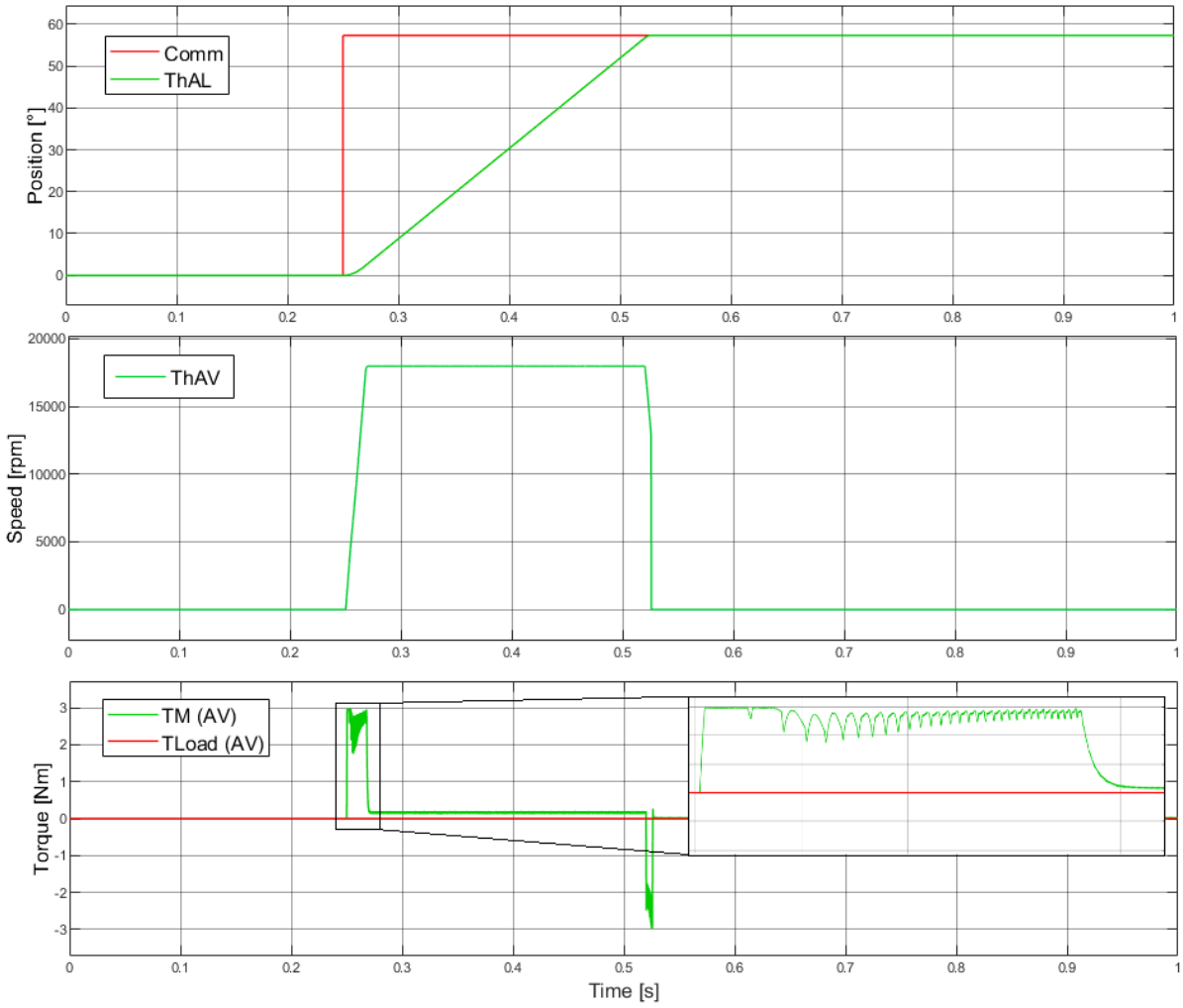

Figure 5.1 - Step Response in non-faulty no-load conditions.

In Figure 5.2 it is shown the current vs. time graph with equivalent filtered and non-filtered currents and reference current. Note that the equivalent nonfiltered current increases to reach the reference current commanded signal and by the time it reaches it, it decreases further due to thermal effect

on winding resistances. Once the motor has reached its maximum speed the currents settle to a value need to counteract the viscous and dynamic friction.

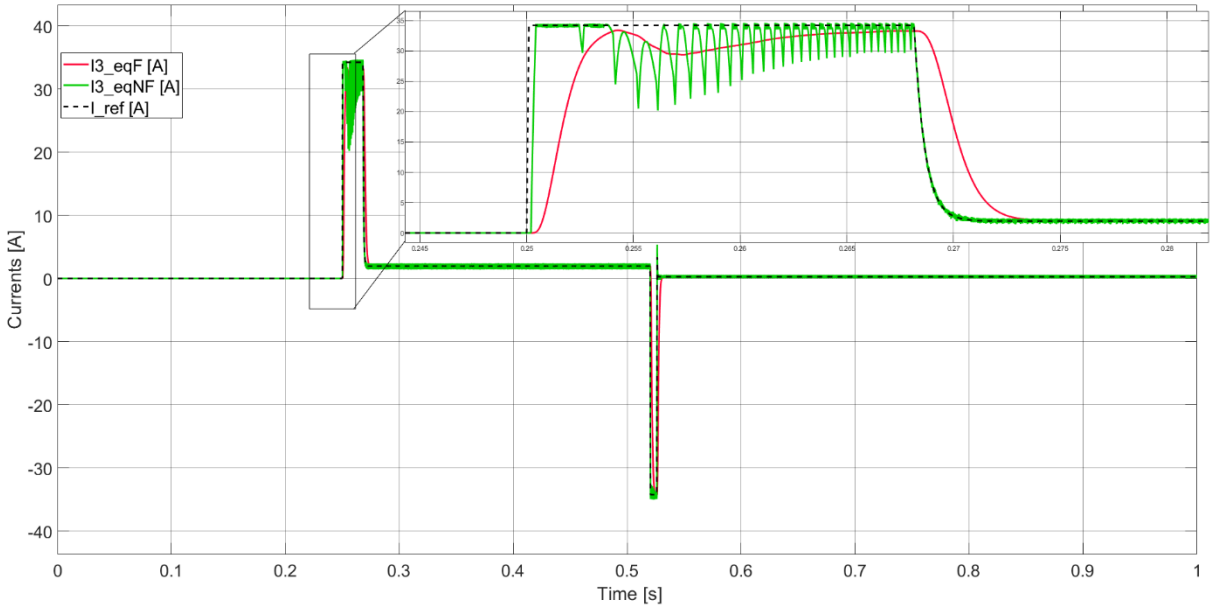

Figure 5.2 - Step Response in non-faulty no-load conditions (Currents)

In figure 5.3 it is shown the temperature graphs vs time for stator case and the three different windings. Note that the 3 windings have a faster dynamic response compared to the stator. This reflects the time constant values of 23 s vs 1222 s respectively. When the transient phase is settled, the windings and the stator reach thermal equilibrium between them and if the simulation time is long enough, they are observed to reach thermal equilibrium with the environment. If a signal needs to be chosen to perform in a prognostic algorithm it needs to be the winding temperature since it has a faster dynamic with respect to the stator temperature, representing the thermal situation in a more responsive way. Most of the BLDC motor manufacturer already offer the option to mount thermal probes in every motor phase iron core or directly on the winding insulation polymer.

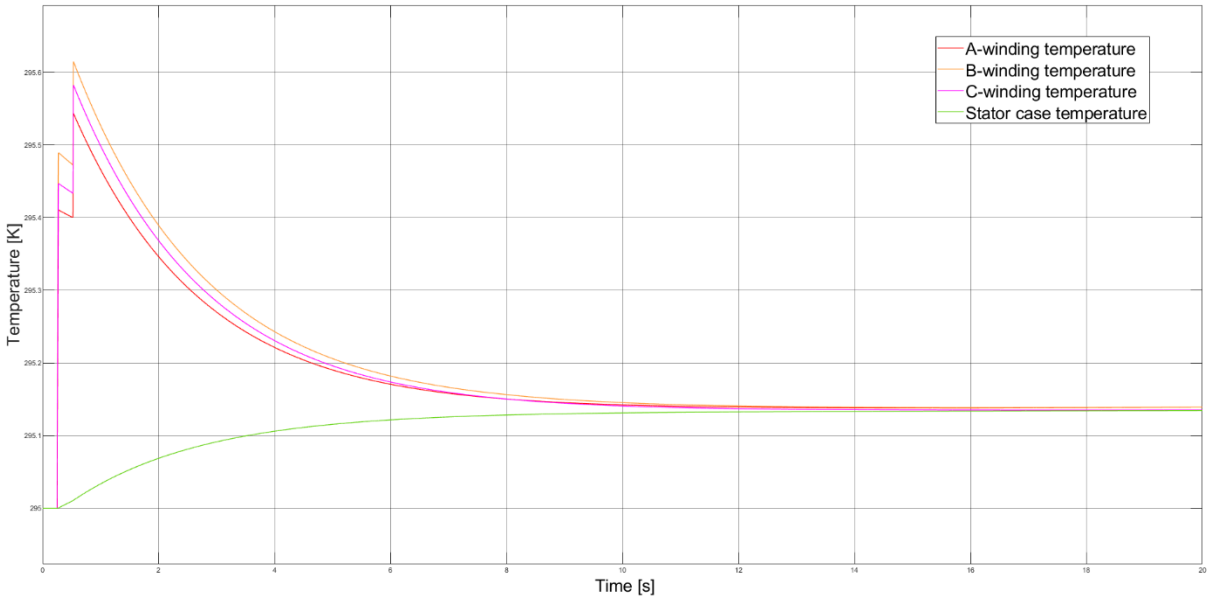

Figure 5.3 - Step Response in non-faulty no-load conditions (Temperature)

5.1.2 Chirp command

A chirp command with no external loads is applied. Amplitude is 0,005 rad and target frequency of 15 Hz is reached after 5 s of simulation. As shown in Figure 5.4, the command input is followed with a small phase lag. The effect of friction can be observed when the velocity value reaches and crosses the zero value. At every speed crossing a small position error is introduced and the effect can also be seen directly on position graph, looking at the “crests” of the function which results flattened. The more the friction is increased due to wear the “flatter” this curve appears.

As in the step input case, the torque has visible ripples due to the PWM switching logic; the same behaviour is observable on the equivalent non-filtered current signal (Figure 5.5). In the current graph is it also visible the peak in current due to backlash (near speed reversal). The control logic in this case is commanding a higher reference current value to catch up with increasing position error due to transmission backlash.

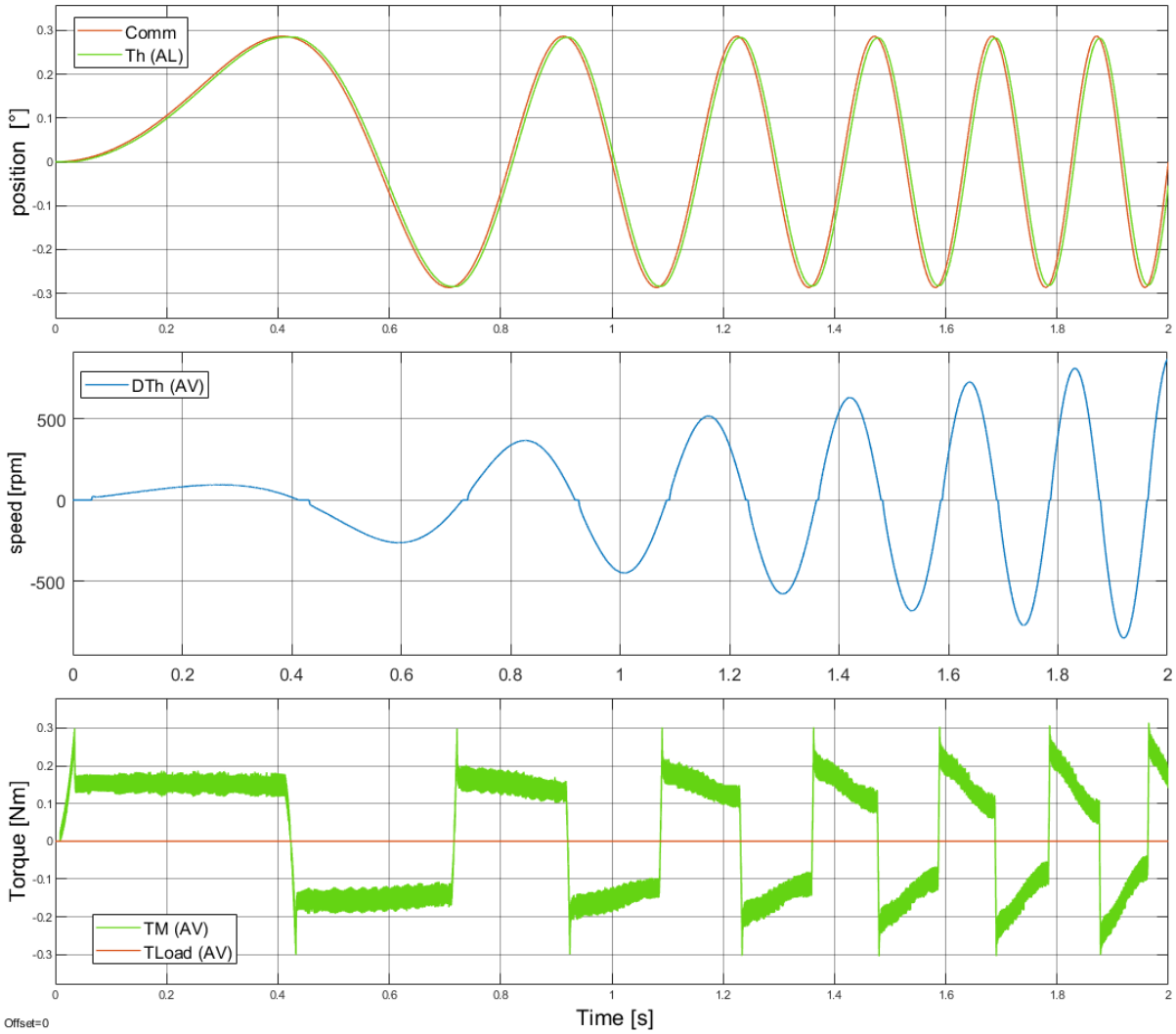

Figure 5.4 - Chirp Response in non-faulty no-load conditions (Position- Speed - Torque)

In Figure 5.6 the temperature graph it is shown: in this case due to low current values the temperature in the windings doesn't changes quite a lot in value. This type of command is main used to evaluate friction and backlash faults, that are more evident for slow speeds of the motor. For this reason, a low value of chirp command amplitude was chosen.

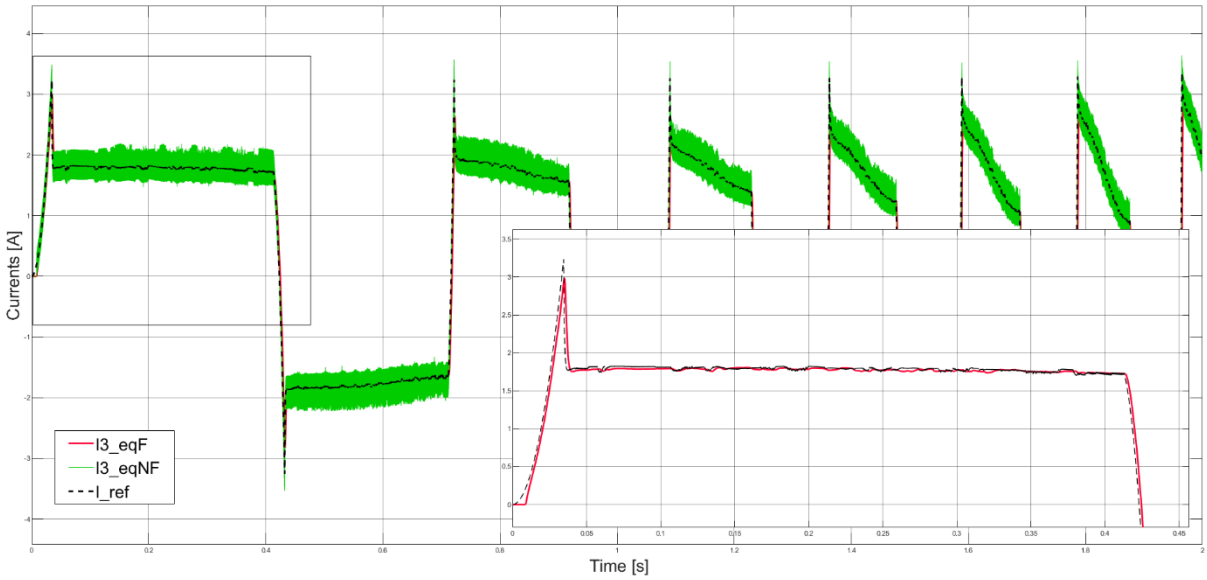

Figure 5.5 - Chirp Response in non-faulty no-load conditions (Currents)

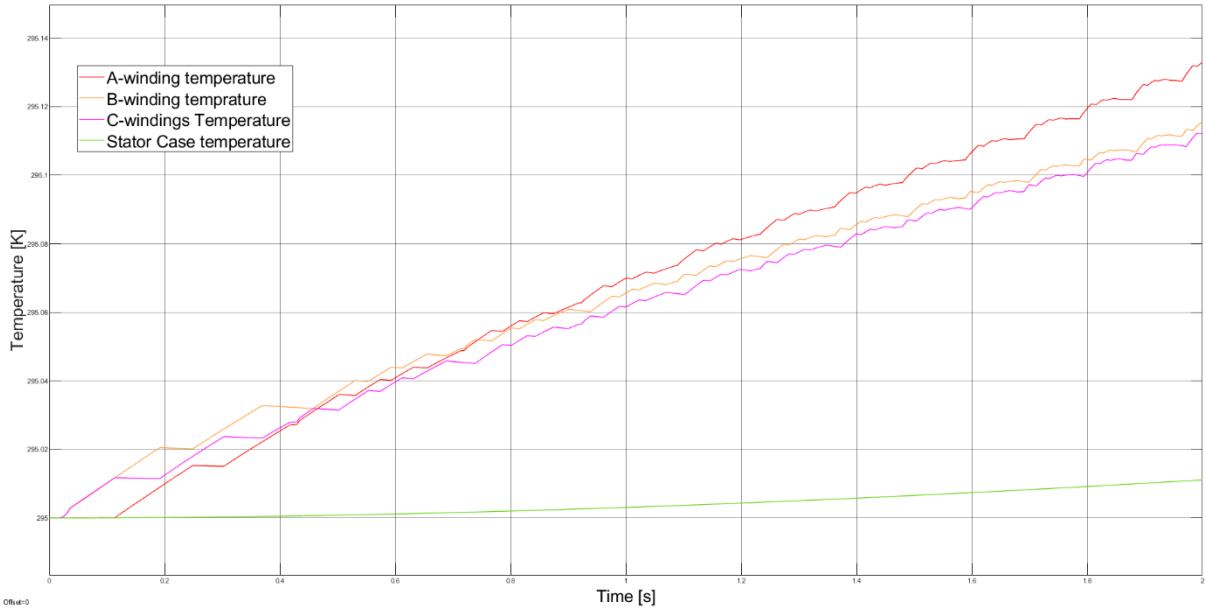

Figure 5.6 - Chirp Response in non-faulty no-load conditions (Temperature)

5.2 Nominal: No fault – Secondary surface Load

In Figure 5.7 it is shown the response to a step command with a constant external load. This load condition is scaled on the maximum value of torque load for a Secondary-like flight surface (Flaps), which is the motor stall torque T_0 (see Chapter 4) divided by *1,5*. Similar results can be obtained using a Primary-like flight surface (Ailerons); in that case the maximum torque would have been the motor stall torque divided by 2. These load condition, as the no-load condition aren't the same as the ones the EMA is subjected during the flight, since that load would be at least proportional to the surface deflection and other geometry, stream and flight parameters. The load is assumed to be a static constant load applied on the slow shaft of the surface, having the same constant value disregard of the direction of motion. This might be a test loads applied on a test bench where a weight is placed on the surface mechanism. A more realistic way of modelling the load would need at least the flight data from the aircraft with the data from a torque sensor on the hinge.

5.2.1 Step command

As shown in Figure 5.7, the EMA in this load conditions starts to lose the position at around t = 0,035 s, after the motor (AV), driven by the initial closes the gap given by the backlash of the transmission. The motor started to move under the effect of the torque load, the control electronics immediately start to break this initial acceleration, but only when a position error is detected (once the backlash is filled) it starts to slow the motor down. Note that the position error is only recovered once the step command is applied (at t = 0,25 s) i.e. after the error magnitude can be managed by the Proportional only control logic. The same observation can be made for the end of the transient (nearly at t = 0,55 s).

Speed wise, considering also the response to a step command under no load conditions of the previous sections, it is shown the slower transitory phase, since the EMA has less “net” torque available for acceleration. In case of the simulation of a Primary flight surface, the actuation speed would have been a main requirement to be met, since the response of a surface needs to be the same under all the load conditions in the flight envelope. Note that the acceleration and deceleration of the motor span across time intervals of different length, this is happening due to the load torque acting as a brake on the shaft. This would have happened even in a more realistic load condition, only, with a more “rounded” stop of the motor.

The torque graph reflects all the consideration that are already been made for position and speed. The longer the acceleration phase (the time it takes to the motor to reach the max speed), the longer the three phases are heated by the controlled currents and the higher the temperature. Note that the more realistic the load conditions are, the more the thermal model is suitable to be used in prognostic algorithms.

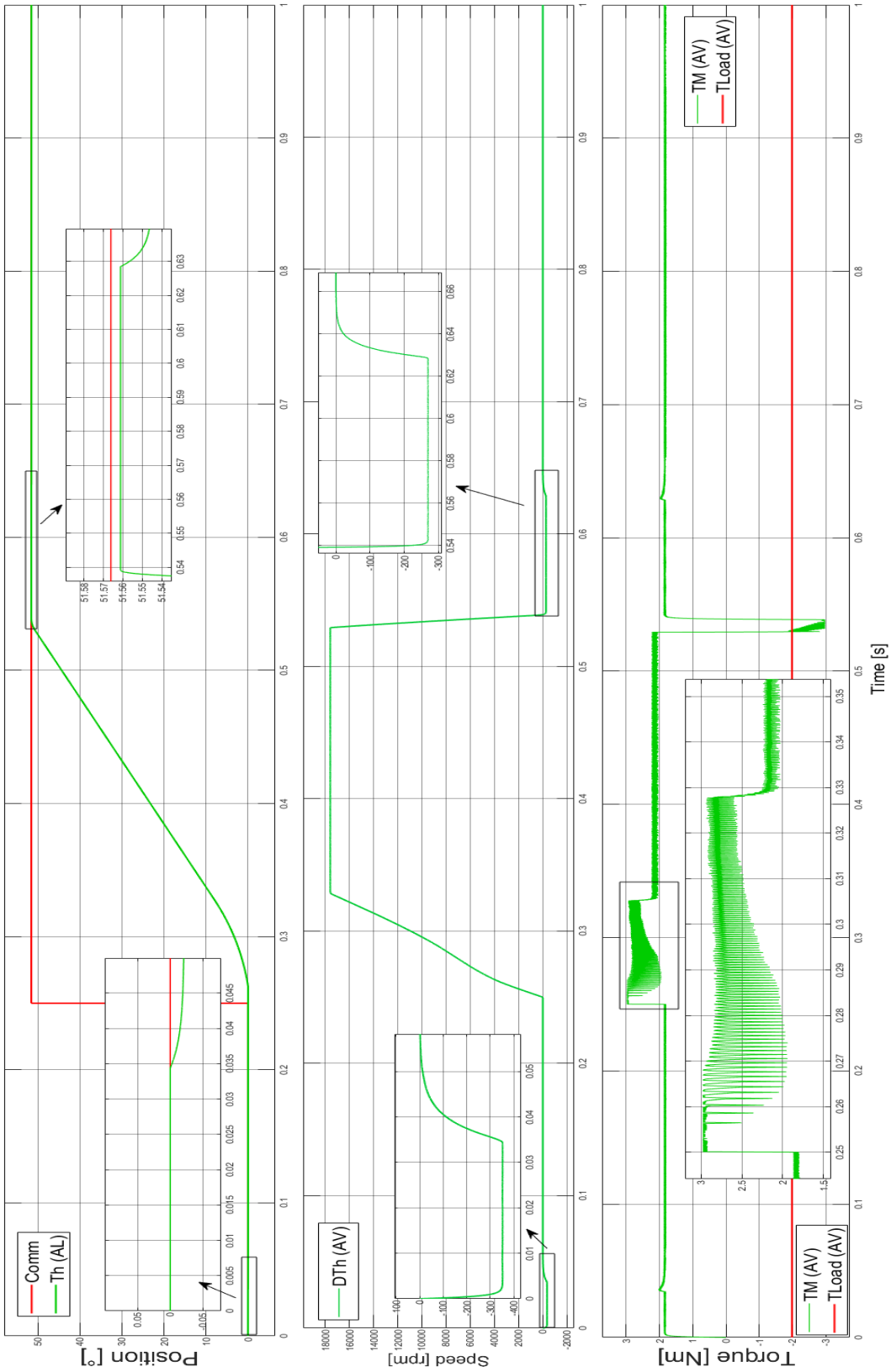

Figure 5.7 - Step Response in non-faulty - Secondary (Flap-like) load conditions (Position, Speed, Torque).

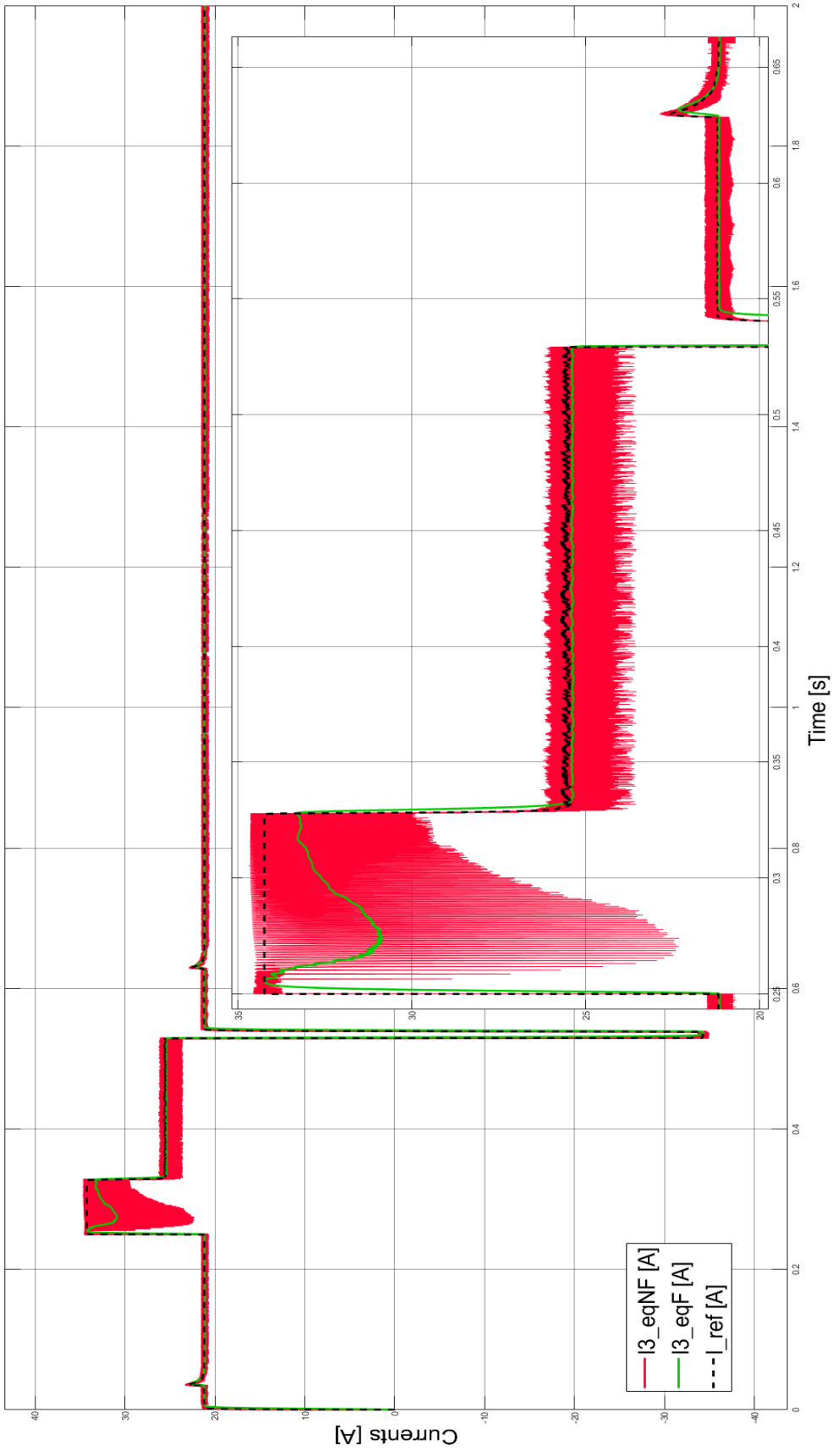

Figure 5.8 - Step response in non-faulty Secondary type (Flap-like) conditions (Currents).

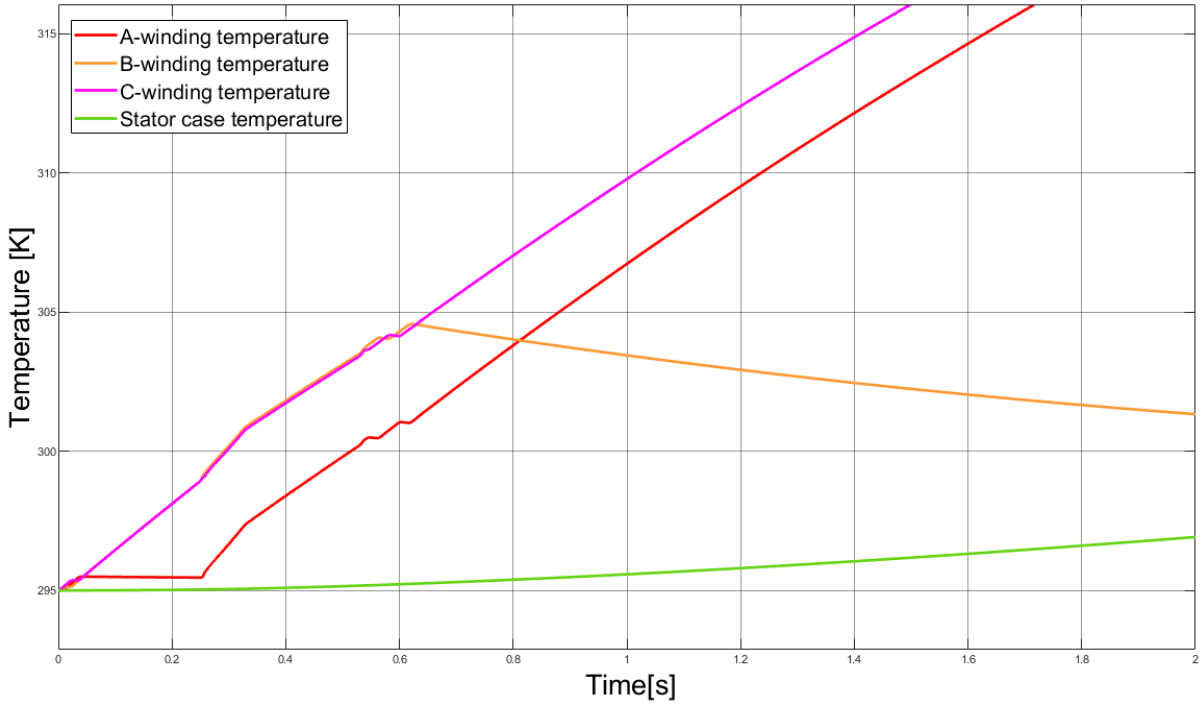

Figure 5.9 – Step Response – Secondary (Flap-like) Load conditions (Temperature)

In temperature graph is shown what happens to the temperature in the model (it also reflects a real motor behaviour) when there's the need to output a torque at zero speed: the temperature of the winding of phase A is the one that remains unpowered during the first "stall" of the motor (nearly between t = 0,05 s and t = 0,3 s). The hall sensor block in the BLDC motor model doesn't read a switch in the variables that indicates that the rotor is moving, so it continues to keep feed the same two phases with current, increasing in this way their temperature by nearly 5 degrees respect to the phase that is left unpowered.

The same behaviour is repeating from t = 0,6 s, in this case the B-phase is the one left unpowered, going in equilibrium with the stator case. Not that if a motor were to be chosen for an application and it shows this temperature trend, there would be a failure in the system within a few seconds since the maximum winding temperature would be reached within a few seconds, assuming a max temperature of T_{max} = 125 °C (see the motor datasheet in Chapter 2).

5.2.2 Chirp command

The response to chirp command in Figure 5.10 shows that every dynamic of stop/start at zero speed crossing is even more stressed under a constant load condition. The position graph shows the same “flattened” peaks and valleys, but with a longer duration in time due to the slower response of the motor when it have to compensate for the load torque and with a faster response (so a shorter “flat” zone) when the load torque acts in “accordance” with the motor rotation.

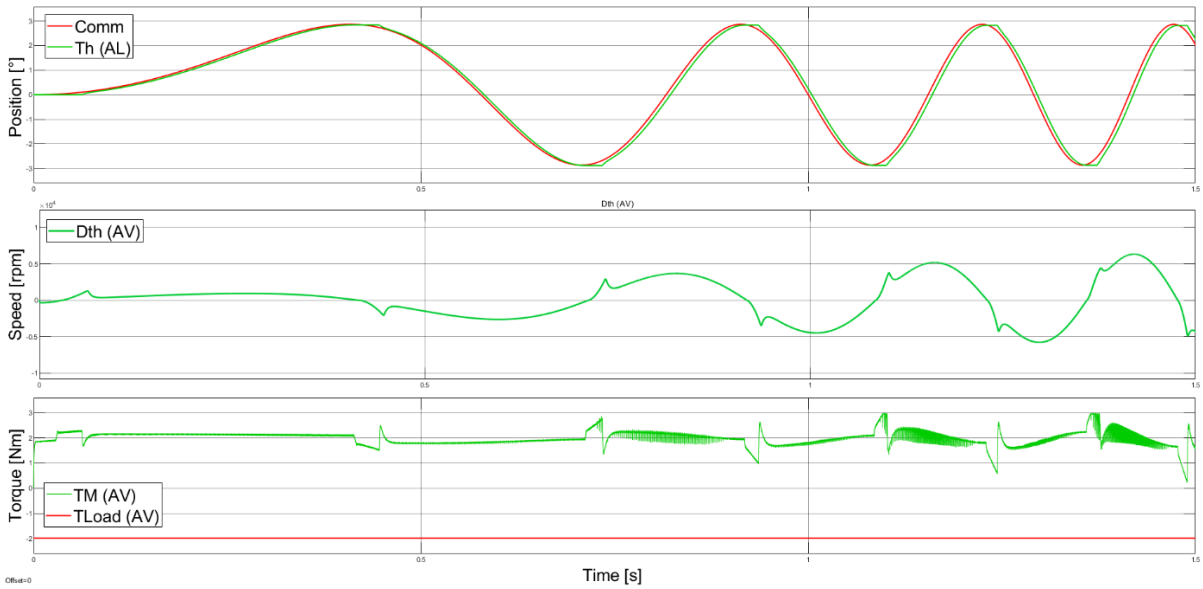

Figure 5.10 – Chirp response - Secondary type (Flap-like) conditions (Position- Speed - Torque).

Also, the temperature graph shows the same initial trend, but with a higher value faster dynamic, since the currents are “constantly” (according to PWM switching) flowing in the three-phase motor, to produce the torque needed to counterbalance the load. The absolute value of the currents is also higher, and this means that the power loss due to Joule effect is also higher, therefore raising the temperature value.

Figure 5.11 – Chirp response in non-faulty Secondary type (Flap-like) conditions (Currents).

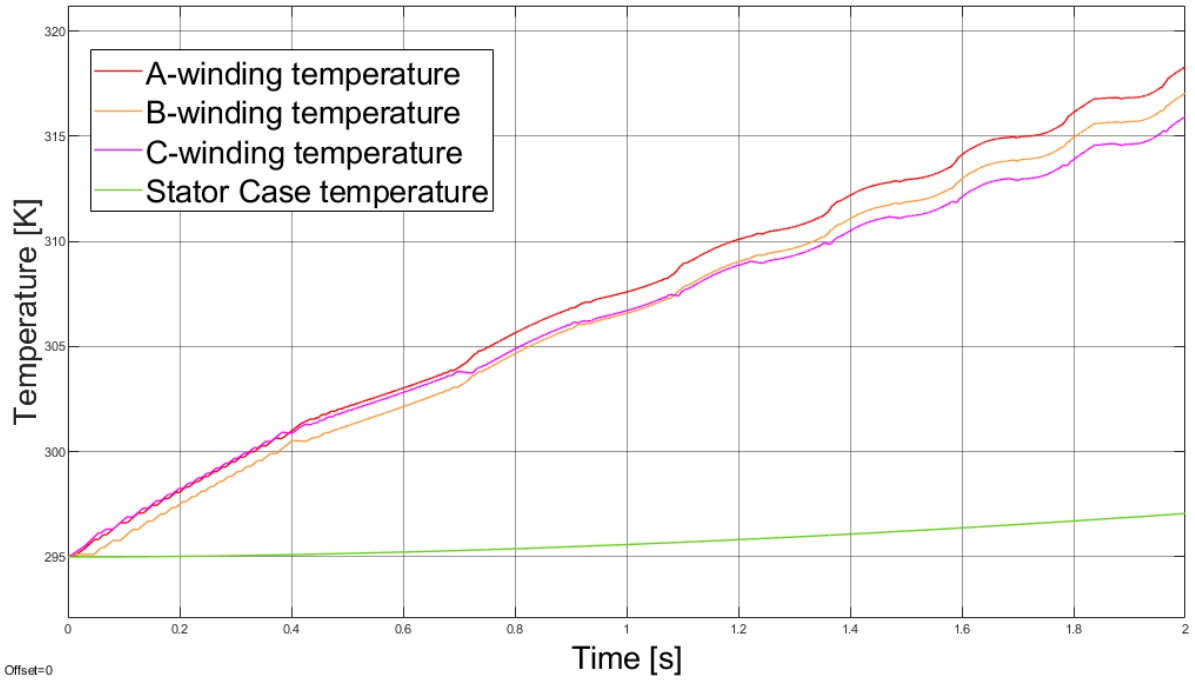

Figure 5.12 – Chirp response in non-faulty Secondary type (Flap-like) conditions (Temperature).

6.Conclusions and Future Works

In this work, a simple but functional dynamical thermal model for a three-phase Brushless DC motor is integrated successfully in a high-detailed Electro Mechanical Actuator model for aeronautical applications. The thermal model considers only one type of power loss, i.e. only one thermal source and its coupling with the electrical model. From literature this is the main but not the only thermal effect that is influences a motor performance. To gain confidence with the EMA technology and raise its level of readiness, it would be fundamental to implement the other type of power losses and their effect on electro-magnetic network (e.g. effect of temperature on motor torque and Back-EMF) of the motor. Another type of analysis might be an evaluation of RUL of the component based on its temperature history, since they are directly linked through the deterioration of the insulation material of the windings (see Chapter 4 on motor thermal classes).

In order to further validate the model, given the uncertainties due to the unavailable motor parameter from the manufacturer, a test bench for experimental measures would be needed. On the test bench the temperature could be measured from each motor phase and compared to simulation results to assess the error on the mass estimation and to evaluate the level of detail needed by the model to be useful as a reference model in a prognostic algorithm. Also, with a test bench for thermal measures, a more complete model of motor can be built, extending the thermal RC network to mimic the real motor. An alternative would be to keep a simple model but with thermal resistance values derived from experimental measures.

A further step to validate the EMA model for aeronautical applications would be the creation of a load block that simulate real in-flight hinge torque for the surface. This can be done either with flight data and the direct measure of the hinge moment around a surface or with a test bench in a wind tunnel.

On the other hand, prognostic and health management has the goal of estimating a component RUL by evaluating in advance a slowly progressing fault. A sudden fault is not of interest for prognostic since it can't be foreseen. The lack of the need to make a prompt estimate of a system health status makes possible to perform the same estimate during any time of the flight operation, even during on-ground operations, since, as already mentioned a systems' conditions do not change significantly during a single flight. For these reasons a pre-flight check-up can be simulated by setting external load on the surface to zero.

Before using this model in a prognostic algorithm, all available fault modes need to be further tested, to ensure that they are still visible and identifying the variable to be used in a fault isolation algorithm. To proceed with the development of a fault isolation algorithm, be it Artificial Neural Networks, Genetic Algorithms or other, a reference model needs to be built and tested. The model has to resemble the high fidelity/detail model but needs to be optimized to perform with a fault isolation method.

Bibliography

[1] Paolo Maggiore – Notes from *"Sistemi di Bordo Aerospaziali",* A.A. 2012-2013.

[2] Paolo Maggiore, Matteo Davide Lorenzo Dalla Vedova – Notes from *"Modellazione, simulazione e sperimentazione di sistemi aerospaziali"*, A.A. 2015/2016.

[3] https://www.f15sim.com/operation/f15_hydro_mech.html

[4] Faulhaber "Technical information", 13th edition 2019 (www.faulhaber.com).

[5] Paolo Maggiore, Matteo Davide Lorenzo Dalla Vedova, Pier Carlo Berri - *"Genetic algorithms for Prognostic of Electromechanical Actuators",* 2016.

[6] Manuela Battipede, Matteo Davide Lorenzo Dalla Vedova, Paolo Maggiore and Simone Romeo, *"Model based analysis of precursors of electromechanical servomechanisms using an artificial neural network",* 2015.

[7] Dave Staton, Livio Susnjic *"Induction motor Thermal Analysis",* 2009.

[8] Dave Staton, Aldo Boglietti, Andrea Cavagnino *"Solving the More Difficult Aspects of Electric Motor Thermal Analysis",* 2014.

[9] Xiaofeng Ding, Madhur Bhattacharya, Chris Mi *Simplified Thermal Model of PM Motors in Hybrid Vehicle Applications Taking into account Eddy Current Loss in Magnets",* 2010.

[10] Cleve Molder, Mathworks™, *"Ordinary Differential Equations – Mathematical Models in many different fields.",* October 2, 2011.

[11] Lawrence F. Shampine, Mark W. Reichelt, Jacek A. Kierzenka "*Solving Index-1 DAEs in MATLAB and Simulink",* February 22, 1999.

[12] F.Z. Zhou, J.X.Shen, W.Z.Fei, "*Influence on rotor eddy-current loss in high speed PM BLDC Motors",* Febrary 10, 2017, College of Electrical Engineering, Zhejiang University.

[13] Allan R. Hambley "*Elettrotecnica*", 4th Edition, 2013.

[14] IEEE 117-2015, "*IEEE Standard Test procedure for thermal evaluation of systems of insulating materials of random-wound AC Electric Machinery",* Published 2016-05-06.

[15] IEEE 101-2015, "*IEEE Guide for the Statistical ANlysis of Thermal Life Test Data",* Published 1988-12-31 (Reaffirmed 2010-12-08).

[16] C.D.Fuerst-E G.Brewer, "*High remanence rapidly solidified NdFeB: Die-upset magnets(invited)",* Journal of applid physics nr 73 (10), 1993.

[17] J. Pyrhonen, T.Jokinen, V. Hrabovcova, *"Design of rotating Electrical Machines",* 2009.

[18] C. Lungoci, D.Stoia *"Temperature effects on torque production and efficiency of motors with NdFeB",* 2008.

[19] MathWorks™, "MATLAB Documentation" ww.mathworks.com/help/.